Rab11FIP1 maintains Rab35 at the intercellular bridge to promote actin removal and abscission

Nicholas V.G. Iannantuono[a] and Gregory Emery[a,b,c]

[a] Institute for Research in Immunology and Cancer (IRIC), Université de Montréal, Montréal, Québec, Canada.

[b] Department of Pathology and Cell Biology, Faculty of Medicine, Université de Montréal, Montréal, Québec, Canada.

[c] Lead author, correspondence should be addressed to Gregory Emery (gregory.emery@umontreal.ca).

Abstract

Cytokinesis occurs at the end of mitosis/meiosis wherein the cytoplasms of daughter cells are separated. Prior to abscission, an intercellular bridge containing the remaining furrowing machinery, mitotic spindle and actin cytoskeleton connects the two daughter cells. To remove this actin and allow for separation of daughter cells, Rab35 vesicles, loaded with the actin oxidizer MICAL1 and the inositol polyphosphate 5-phosphatase OCRL are recruited to the midbody in a fine-tuned spatiotemporal manner. Importantly however, the means by which these vesicles are recruited is currently unclear. Here, we demonstrate that Rab11FIP1 is recruited to the midbody after Rab35 to scaffold it at the bridge and maintain Rab35 in this region. In the absence of Rab11FIP1, Rab35 dramatically drops from the midbody, inducing defects such as cytokinetic delays and binucleation due to actin overaccumulation at the intercellular bridge, defects which can be rescued with Latrunculin A treatment. Importantly, we show that Rab11FIP1 is critical for Rab35 function in actin removal prior to cytokinesis.

Introduction

Cytokinesis occurs at the end of mitosis/meiosis wherein the cytoplasms of daughter cells are separated, giving rise to two independent cells (Frémont and Echard, 2018, Gatta and Carlton, 2019, Holder et al., 2019, Peterman and Prekeris, 2019, Vietri et al., 2020). Just prior to this abscission, daughter cells remain attached by an intercellular bridge that contains the remnants of the furrowing machinery and an array of cytoskeleton components, including the mitotic microtubule spindle and actin cytoskeleton (Frémont and Echard, 2018, Peterman and Prekeris, 2019, Echard, 2008, Klinkert and Echard, 2016, Kouranti et al., 2006). The removal of this filamentous actin prior to abscission has been a field of active research over the past decade as its ineffective removal has been tied to deficient abscission, which in turn has been linked with diseases such as Lowe-Syndrome and cancer (Carim et al., 2019b, Carim et al., 2019a, Festa et al., 2019, Bökenkamp and Ludwig, 2016, Erneux et al., 2016, Cauvin et al., 2016, Sugimoto et al., 2014, Vicinanza et al., 2011, Chesneau et al., 2012).

In fact, the removal of this actin has been linked with very precise modulation of the intercellular bridge lipid composition by the small GTPase Rab35 (Frémont and Echard, 2018, Kouranti et al., 2006, Dambournet et al., 2011). Rabs are small GTPases that regulate different stages of intracellular trafficking. These proteins oscillate between inactive and active states, where they are thought to bind downstream effectors and modulate cellular functions pertaining to trafficking such as vesicle fusions, motility and docking. Rab35 has been linked to several functions, most notably fast recycling to the plasma membrane (Klinkert and Echard, 2016, Cauvin et al., 2016, Chesneau et al., 2012), but most recently its linchpin role in cytokinesis has been at the forefront. Indeed, Rab35 has been shown to recruit both MICAL1 (Frémont et al., 2017) and OCRL (Cauvin et al., 2016, Dambournet et al., 2011, Frémont et al., 2017, Kouranti et al., 2006). MICAL1 is an actin oxidizing enzyme that causes actin depolymerization, while OCRL is a PI(4,5)P2 phosphatase that helps to detach any remaining furrowing machinery and actin nucleators. This alleviates the barrier of actin that has been shown to physically impede ESCRT-III polymerization, however the means by which Rab35 is specifically recruited after telophase to the intercellular bridge in unclear.

Of note, as said earlier, Rabs act through different effectors and a specific group of Rab11 effectors, namely Rab11FIPs (henceforth named FIPs) have been well characterized as linking Rab11 vesicles with molecular motors (Baetz and Goldenring, 2013, Carson et al., 2013, de

Renzis et al., 2002, Eva et al., 2010, Fan et al., 2003, Fan et al., 2004, Jin and Goldenring, 2006, Jing et al., 2010, Lall et al., 2015, Li et al., 2014a, Li et al., 2014b, Lindsay and McCaffrey, 2005, Lindsay and McCaffrey, 2004, Moore et al., 2004, Nedvetsky et al., 2007, Neto et al., 2013, Peden et al., 2004, Rainero et al., 2012, Sechi et al., 2014, Willenborg et al., 2011). FIPs come in two classes, namely the FIP1, FIP2 and FIP5 of the Class I FIPs and FIP3 and FIP4 of the Class II FIPs. Class I FIPs have been associated with various trafficking events such as the recycling of different proteins to the plasma membrane such as GLUT4-containing vesicles (Bruno et al., 2016), the water channel protein AQP2 (Nedvetsky et al., 2007), the chemokine receptor CXCR2 (Fan et al., 2003, Fan et al., 2004) and different integrin complexes, most notably α5β1 (Eva et al., 2010, Hwang et al., 2017, Rainero et al., 2012). As for Class II FIPs, both FIP3 and FIP4 have been shown to play key roles during cytokinesis where they couple Rab11 and Arf6 at the intercellular bridge during cell division (Ai and Skop, 2009, Chesneau et al., 2012, Takahashi et al., 2011). Of note, mammalian Class I FIPs have not currently been formally linked to cytokinesis. Nevertheless, we have shown in a prior study, that the sole Drosophila Class I FIP, Rip11 localizes to the ICB and its depletion leads to cytokinesis defects in a Rab11-independent manner (Laflamme et al., 2017).

Here, we present our data strongly suggesting that FIP1 acts as an atypical molecular tether that serves to maintain Rab35 levels elevated in the ICB prior to abscission and that its depletion leads to dramatic drop-off of Rab35. We show that FIP1 depletion leads to similar phenotypes to the depletion of Rab35 including cellular binucleation and cytokinesis delays and polarity inversion in 3D cultures due to overaccumulation of actin and subsequent cytokinesis failure. Finally, we show that FIP1 depletion can be rescued entirely with a low dose of Latrunculin A to artificially reduce actin levels, similarly to what was observed in Lowe-Syndrome patient cells.

Results

FIP1 is required for timely cytokinesis completion

In order to examine the function of Class I FIPs on mitosis, we first individually depleted the three FIPs of class I, hereafter named FIP1, FIP2 and FIP5, in U2OS cells (Fig. 1A). The knockdown of FIP1, FIP2 and FIP5 did not induce any overt phenotypes with regards to the cytoskeleton nor cause any other gross morphological phenotypes (Fig. 1B). Nevertheless, a

subtle (~7%) but significant increase in binucleated cells could be observed in cells knocked down for FIP1 (Fig. 1C). Moreover, cumulative depletions of different FIPs never caused synergistic effects, always remaining at a similar binucleation to FIP1 depletion alone (Fig S1A). It is of note that we could not measure binucleation in the triple knockdown as significant cell death was quickly induced over the first three days. Nevertheless, to ensure that this phenotype was not cell line specific, we performed FIP1 knockdown in a variety of different cell lines. Our results showed that in all cell lines, with the exception of HeLa cells, the silencing of FIP1 induced cell binucleation to varying degrees, with U2OS showing the most prominent effects (Fig S1B).

We next sought to understand the mechanism by which cellular binucleation was induced. For this, we first examined the state of telophase cleavage ring furrowing, as unstable furrowing often leads to binucleation. We therefore monitored one of the major regulators of cytokinesis, the centralspindlin component MKLP1, whose functions include tethering the mitotic spindle to the plasma membrane for proper formation of the midbody after telophase. Indeed, MKLP1 staining showed no observable differences between control and FIP1-depleted cells (Fig S1C). Furthermore, we expressed the RhoA-binding-domain-of-anillin as a proxy for RhoA activation and localization and found no difference between control and FIP1-depleted cells (S1C). Upon closer examination, we observed that FIP1 depletion induced an increase in the percentage of cells bound by acetyl-tubulin-positive bridges (Fig. 1D) as well as a decrease in the amount of those bridges that displayed secondary ingressions (Fig. 1D). These results strongly suggest that FIP1 depletion causes an abscission delay. Indeed, our measurements of the time between telophase and mitotic spindle severing (Fig. 1E) indicate that while control cells on average take 170 minutes to complete cytokinesis, cells depleted for FIP1 require 328 minutes (Fig. 1E, S1D), indicating a cytokinesis delay. Long-term depletion of FIP5 yielded high cell death post 72 hours, thus we excluded this protein from further analysis. As expected, knockdown of FIP2 induced no cytokinesis delay (Fig. 1E, S1D). To explore what might be causing this cytokinetic delay, we first examined the localization of FIP3, an important player in the delivery of Rab11-positive endosomes to the ICB, as well as the ESCRT-III component CHMP4B. Of note, whether looking at early recruitment to intercellular bridges harboring no secondary ingressions, or looking at late ICBs displaying clear secondary ingressions, we could not observe any difference in the levels of FIP3 or CHMP4B suggesting that FIP1 depletion does not impede the

ability of these proteins to localize to the intercellular bridge (Fig S1E). There are different isoforms of FIP1, namely FIP1A, FIP1B and FIP1C. Thus, we sought to determine which of these isoforms was required in cytokinesis. To this end, we established stable cell lines expressing GFP-FIP1A, GFP-FIP1B and GFP-FIP1C (Fig. 1F). It is of note that our siFIP1 targets the 3' UTR, and thus, it does not affect the expression of our exogenous constructs. When these cells were subjected to FIP1 knockdown, both FIP1B and FIP1C, but not FIP1A expression rescued both binucleation and cytokinesis timing (Fig. 1G, 1H and S1D), suggesting that either FIP1B or FIP1C are redundantly required for timely cytokinesis completion.

FIP1B and FIP1C localize to the midbody, abscission site and daughter cell:cell interface during mitosis

Since FIP1B and FIP1C rescue the binucleation and cytokinesis timing phenotypes observed during FIP1 knockdown, we investigated the specific localization of the different FIP1 isoforms (Fig. 2A) during mitosis using live-cell imaging on our stable cell lines. Both FIP1B and FIP1C localize to vesicular structures in most of interphase, while FIP1A demonstrates mostly cytoplasmic staining (Fig. 2B). Interestingly, neither A, B nor C showed any distinct localization during mitotic prophase, metaphase and anaphase. Upon entry into telophase, FIP1B localization changed drastically towards the extremity of the mitotic spindle between both daughter cells, a localization that remained stable throughout telophase progression until a sudden shift towards the middle of the spindle just prior to abscission with a gradual pullback to the sides of the abscission site after abscission had occurred, as represented by the line scans below each image (Fig. 2B). FIP1C localization was very similar to that of FIP1B, as can be seen in (Fig 2B), wherein FIP1C localizes to both extremities of the spindle during telophase and just after abscission. Upon entry into G1, both FIP1B and FIP1C have very similar localization. As for FIP1A, it remains cytoplasmic throughout mitosis and does not show specific localization to any clear mitotic component, be it the spindle or abscission site. These results suggest that FIP1B and FIP1C are recruited to the ICB during the end of mitosis.

Rab11FIP1 interacts with Rab35 via both its N and C-terminus

Since our results suggest that FIP1B and FIP1C have activity in cytokinesis, we sought to identify a cargo they may be trafficking during this phase. To do this, we first examined the recently published Bio-ID interactome of FIP1 available in the online database https://cell-map.org/ (Fig.3A). As expected, Rab11A is reported as the strongest hit. In addition, there are several proteins involved in endocytic recycling such as STX7, STX6, RAB9a, CAV1 and RAB5A. Most interestingly, Rab35 was detected with a near perfect SAINT score of 0.98 and this protein has recently been strongly tied to cytokinesis defects that are reminiscent of the phenotype we observed in FIP1 knockdown. As such, we examined FIP1 binding with Rab35. Firstly, we performed immunoprecipitations of exogenous constructs for each isoform of FIP1 using different Rabs as baits. As expected, all FIP1 isoforms interact strongly with both Rab11a and Rab11b (Fig. 3B). Furthermore, we observed interaction between Rab35 and all three isoforms of FIP1. We also tested another known interacting Rab, namely Rab14 (Lall et al., 2015, Qi et al., 2013) despite it not appearing in the BioID analysis and could also observe interaction with all three isoforms of FIP1 (Fig 3B). Strikingly, in (Fig. 1F and 3B), the FIP1C exogenous construct appeared as a double band which both interact with Rab11a and Rab11b but only the upper band seems to interact with Rab35 or Rab14. We also examined FIP1 interaction with a panel of other Rabs, namely Rab1a, Rab5, Rab6a, Rab10 and Rab13. When performing immunoprecipitations of either exogenous FIP1B or FIP1C, we could only observe interaction with exogenous Rab11 and Rab35 (Fig. S2A, left and right). As expected, binding between FIP1B/C and Rab11 is stronger than with Rab35. Next, we developed different N-terminal deletion constructs of FIP1B to map the domain of interaction with Rab35. As expected, the Rab11-binding domain (RBD) of FIP1 could interact with Rab35 (Fig. 3C, left) confirming what has been published in the literature on the promiscuity of the FIP1 RBD (binding to Rab4 and Rab14) (Qi et al., 2013, Lall et al., 2015). Surprisingly, when we tested if Rab35 could bind other domains of FIP1, we found that while binding to the central domain (108-1211) was barely detectable, Rab35 interacted strongly with the C2 domain of FIP1 (Fig. 3C, right). As the C2 domain is absent in FIP1A, we hypothesize that this binding might confer the specific activity of FIP1B and FIP1C to Rab35. This correlates with the temporal localization changes observed in FIP1B and FIP1C that are absent in FIP1A (Fig. 2B). Furthermore, as many studies and crystal structures have shown FIPs form homodimers, we verified if these two domains can dimerize

with the full length of FIP1 and indeed, both the C2 and RBD can dimerize with full length FIP1 (Fig. S2B) while the middle domain showed poor ability to dimerize with full length FIP1. Crystal structures have shown that FIP1 RBD domains can dimerize (Lall et al., 2015) but it is unclear what function a C2 domain dimer might have. We next sought to determine if FIP1 could act like a Rab35 effector. For this, we performed a similar experiment to that of (Fig. 3B), where we pulled down Rab35 WT and looked at FIP1 binding, but this time we also used Rab35 catalytically active (QL) and dominant negative (SN) and looked at the binding of endogenous FIP1. Interestingly, these results suggest that FIP1C isoform can bind to all variants of Rab35 but showed a preference for Rab35 dominant negative (Fig. 3D). The binding between FIP1B and Rab35 WT could be observed as well however, due to the high molecular weight and low expression of FIP1B relative to FIP1C, it was difficult to observe endogenous FIP1B binding to Rab35 (Fig. 3D). To this end, we sought to confirm these findings using overexpression conditions whereby both FIP1B, the C2 or RBD domains alone were pulled down by Rab35 WT, QL or SN and these experiments showed that FIP1B and its domains all recapitulate the preference for Rab35SN observed with endogenous FIP1C (Fig. 3E). As both FIP1B and FIP1C contain identical C2 and RBD domains, we believe FIP1 might act as an atypical effector, preferring the dominant negative form of this Rab GTPase (Fig. 3E). This parallels the function of IRSp53, which was very recently shown to also specifically bind the dominant negative Rab35S22N and regulate Rab35 localization (Bisi et al., 2020). The discrepancy between entirely and partially exogenous binding (Fig. 3D-E) might suggest that strong expression of FIP proteins increases binding. Furthermore, the inverse experiment, whereby FIP1B and FIP1C was expressed and co-immunoprecipitated, showed binding to endogenous Rab11 as expected (Fig. S2C), but not to endogenous Rab35. This can be due to this interaction only occurring in a subset of mitotic cells and with only a subset of the total FIP1 protein. As such, it would be difficult to observe in this direction.

Finally, as we have observed interaction between Rab35 and different domains of FIP1 (Fig. 3C, right), in various conditions of overexpression and/or endogenous conditions (Fig. 3C-E and S2A), and as we and others have shown that FIP1 domains can dimerize (Fig. S2B), we sought to investigate if we could observe direct binding between FIP1 domains and Rab35 in vitro. For this we purified the His-RBD domain of FIP1 from bacteria and verified its binding with either empty, GTP-loaded or GDP-loaded Rab11 and Rab35. As expected, FIP1 RBD demonstrates

preference towards Rab11-GTP (Fig. S2D). Interestingly, while it can bind GTP-loaded Rab35, FIP1 RBD shows a clear preference towards the GDP-bound form of Rab35, suggesting that FIP1 RBD:Rab35 binding is direct. This is very reminiscent of IRSp53 preference towards Rab35-GDP, as well as our other data regarding Rab35SN. We also tested the ability of the C2 domain of FIP1 to bind Rab35 but we were unable to observe direct binding with the C2 domain in this context (Fig. S2E). This could be due to in vitro conditions not reflecting the cellular or lipidic environment of the C2:Rab35 interaction, lack of post-translational modifications, or simply that the C2:Rab35 binding is not direct. Taken together, our results suggest that FIP1 activity in cytokinesis might be through Rab35 binding.

FIP1 binding to Rab35 is required for its proper localization during cytokinetic abscission

Our previous work demonstrated that the Drosophila FIP1 orthologue Rip11 function was independent of its Rab11 binding. Here, we sought to discriminate whether FIP1 function in cytokinesis was via its Rab11 binding or its Rab35 binding. Since we determined that similarly to other Rab binding, FIP1 could bind Rab35 via its RBD, we developed mutant constructs of the FIP1 RBD, namely Y1254S (which we published as being able to abrogate Rab11:Rip11 binding while retaining its cytokinesis function), the I1255E and D1256N mutants which were shown to abrogate the RBD function as well as an entire truncation of the RBD domain and tested their ability to bind Rab35 and rescue the cytokinesis phenotypes we have observed. Indeed, as expected all three mutant forms and the RBD truncation were completely unable to bind Rab11b (Fig. S3A). Surprisingly, all these mutant forms could bind Rab35 as strongly as the wild-type FIP1B. While we could not demonstrate a direct interaction in vitro (Fig. S2E) between the C2 domain of FIP1 and Rab35, this result strongly suggesting that in cells the C2 domain (Fig. 4A) can confer sufficient Rab35 binding. Furthermore, although this does not preclude the ability of the C2 domain of FIP1 to bind other Rabs, it strongly suggests that the C2 domain of FIP1 is unable to bind Rab11, as it is present in all of these constructs (Fig. S3A). As such, we established stable cell lines expressing different mutant constructs (Fig. 4B, upper) encompassing the C2 and RBD domains as well as the RBD mutants and verified their ability to rescue the FIP1 knockdown phenotype. By measuring cellular binucleation, our results indicate that despite the ability of the individual C2 and RBD domains to bind Rab35 (Fig. 3C), neither domain individually could rescue FIP1 knockdown-induced binucleation (Fig. 4B, lower). The

ΔC2 construct could also not rescue the phenotype, suggesting that the middle domain linked to the RBD does not function in cytokinesis (Fig. 4B, lower). Interestingly, the ΔRBD and other RBD mutant constructs that all retain Rab35 binding (Fig. 4A) but lose Rab11b binding (Fig. S3A) displayed the ability to rescue binucleation (Fig. 4B, lower), suggesting that FIP1 function in cytokinesis absolutely requires the C2 domain linked to the middle domain. Of note, since FIP1 seems to act as an atypical effector of Rab35, we sought to determine the impact of the loss of Rab35 on FIP1 localization. We addressed this question using GFP-FIP1B full length in the presence or absence of Rab35. We could observe two categories of events, wherein most cells would show strong enrichment of FIP1 to the ICB while the rest showed low to no recruitment of the constructs prior to abscission (Fig. 4C, white arrows). Importantly, we could determine that roughly 70% of control cells showed strong recruitment of GFP-FIP1B to the ICB prior to abscission (Fig. 4C). However, knockdown of Rab35 significantly shifted this balance towards lesser recruitment, suggesting that Rab35 is important for FIP1 recruitment to the ICB prior to abscission. Our results highlight the importance of FIP1 binding to Rab35 via its C2 domain for its activity in cytokinesis and strongly suggest that FIP1 function in this process is entirely independent of its classical Rab11 binding.

FIP1 is required for maintaining Rab35 at the midbody

Due to our results suggesting that FIP1 recruitment may be tied to Rab35, we examined the time delay between their enrichments at both the midbody and the daughter cell:cell interface. By monitoring cells just before (-10 mins) and after telophase (+10 mins) that stably express mCherry-Rab35 or GFP-FIP1B, our results indicate that, on average, Rab35 tends to enrich at both these locations prior to FIP1 (Fig. 5A). We next examined what happened to Rab35 localization upon the loss of FIP1 as the phenotype of its knockdown is reminiscent of Rab35 knockdown (Kouranti et al., 2006, Dambournet et al., 2011, Frémont et al., 2017, Prekeris, 2011, Klinkert and Echard, 2016). Unexpectedly, during FIP1 knockdown (Fig 5B), Rab35 levels at the cell:cell interface were significantly lower than in control (Fig. 5C, bottom left). Most interestingly, Rab35 recruitment to the midbody spiked similarly to control just after telophase, albeit to a lower absolute level compared to control, but promptly dropped-off, roughly 1-hour post-telophase (Fig. 5C, bottom right). This coincides with the time when FIP1 would have

enriched at the midbody (Fig. 5A right). These results suggest that FIP1 might be required for maintaining Rab35 levels elevated at the midbody to achieve a timely abscission.

FIP1 maintenance of Rab35 and its effectors OCRL and MICAL1 at the midbody is required for curbing actin overaccumulation and cytokinesis defects

Past studies have linked Rab35 activity and its two effectors MICAL1 and OCRL to lowering actin levels at the midbody. Indeed, the absence of either Rab35 or OCRL has been linked to an overaccumulation of actin at the intercellular bridge. Thus, we knocked down either FIP1 or Rab35 (Fig. 6A) and verified the ICB actin levels via phalloidin staining. As an endogenous Rab35 antibody, that works in immunofluorescence and that we could validate, was not publicly available, we sought to measure its effector MICAL1's recruitment instead. Our results clearly demonstrate that actin levels are significantly higher in both FIP1 and Rab35 depletions while MICAL1 recruitment is almost entirely absent in both conditions, suggesting that FIP1 might participate in Rab35's ability to recruit its effectors (Fig 6A). Another Rab35 effector, namely the phosphatase OCRL has also been shown to be critical for actin removal prior to abscission (Ben El Kadhi et al., 2012, Dambournet et al., 2011). Indeed, OCRL depletion or mutations that lead to Lowe-syndrome have been linked with actin overaccumulation at the ICB, leading to cytokinesis delays. Here, we depleted OCRL and confirmed the induction of cytokinesis delay (Fig. 6B and S4A). It is of note that in our cell type, OCRL depletion also lead to a binucleation phenotype (Fig 6D). Furthermore, low doses of Latrunculin A, hereafter LatA, treatment has been shown to rescue the phenotype of Rab35 depletion-induced OCRL mislocalization in cell models and in Lowe-Syndrome patient cells (Dambournet et al., 2011). Strikingly, the same dose of LatA that could rescue the OCRL depletion phenotype of binucleation and cytokinesis delay (Fig. 6B-E and S4A-B), could also rescue all the phenotypes induced by FIP1 depletion, strongly suggesting that FIP1 is required for maintaining Rab35 levels at the ICB. Finally, as we could observe FIP1 recruitment along the daughter cell:cell interface (Fig. 4C and 5A), we noted how similar it appears to the recruitment of Rab35 after the first division of Caco-2 cells seeded in 3D cultures (Klinkert and Echard, 2016). In fact, similarly to Rab35 depletion, which was reported to induce polarity inversion in Caco-2 cysts, we observed a similar phenotype in FIP1 knockdown (Fig. S4C), again strongly tying FIP1 function to local Rab35 persistence pre-abscission.

Discussion

Our previous studies exploring how Rip11 functions in cytokinesis lead us to investigate how FIPs of class I might also impact cytokinesis in mammalian cells in a Rab11-independent manner (Laflamme et al., 2017). These results strongly suggest that FIP1 isoforms B and C might retain this evolutionary function in regulating cytokinesis. Importantly, our results suggest that the most important function of FIP1B and FIP1C in this process is through the linking of their C2 domain to their middle domain. While, individually, both the C2 and RBD domains become enriched at the ICB, they do not appear to be functional in cytokinesis. Moreover, our results show that the ΔRBD construct can rescue the phenotype, suggesting that other domains in the middle region might also be important but that the C2 domain in the N-terminus is critical for FIP function in cytokinesis. Indeed, our results demonstrate that both FIP1B and FIP1C, which contain an N-terminal C2 domain (Fig. 2A) known to bind phosphoinositides (Lindsay and McCaffrey, 2004, Nalefski and Falke, 1996, Jin and Goldenring, 2006) , show dramatically different temporal localizations during mitosis to that of FIP1A (Fig. 2B).

Rab35, one of the proteins identified in the FIP1 Bio-ID (Fig. 3A), has been extensively demonstrated to regulate cytokinesis via the recruitment of major players in the steps prior to abscission (Echard, 2008, Prekeris, 2011, Klinkert and Echard, 2016, Chesneau et al., 2012, Cauvin et al., 2016, Dambournet et al., 2011, Frémont et al., 2017, Kouranti et al., 2006). However, these studies have not explored the means by which Rab35 is recruited to the ICB during this process. Here, our data show that Rab35 is tethered to the ICB by binding FIP1, since its recruitment occurs prior to that of FIP1 (Fig. 5D). In other words, FIP1 presence seems to be important for maintaining Rab35 levels at the ICB, as its depletion causes a dramatic drop-off of Rab35 in the minutes following its recruitment (Fig 5C). We believe this leads to the over accumulation of actin and subsequent cytokinesis delays we observed.

In fact, one of the few studies that did explore Rab35 recruitment during mitosis identified that Rab35 regulates apico-basal polarity by regulating AMIS formation in Caco-2 cysts, wherein its depletion induces apical component mislocalization and polarity inversion (Klinkert et al., 2016). However, this was linked to direct binding between Rab35 and PODXL at the apical membrane, thus tethering Rab35 to this location. Our results suggest that FIP1 depletion also induces a similar polarity inversion in this cell-type, to a similar degree to the depletion of Rab35. It would

be interesting to investigate how FIP1 functions in the Rab35/PODXL axis. Indeed, while our data suggests that FIP1 tethers Rab35 to the ICB, the recruitment of Rab35 per se was recently shown to be mediated by IRSp53, which regulate the Rab35:PODXL axis during lumen formation by binding and recruiting Rab35S22N to the AMIS (Bisi et al., 2020). Whether FIP1 participates in this process directly or in parallel will need further study. On a side note, our results in this cell type do not seem to concord with prior research suggesting that FIP5 is important for AMIS formation in a Rab11-dependent manner in MDCK cells, as our results do not indicate that FIP5 has any impact on AMIS formation in Caco-2 cells, however this could be attributed to differences in cell lines and/or lack of complete depletion due to siRNA-mediated knockdowns of proteins in our experiments (Li et al., 2014b, Willenborg et al., 2011).

More specifically, our structure function and biochemical analysis revealed that FIP1 isoforms demonstrate preference for the dominant negative form of Rab35 (Fig. 3D-E and S2D), suggesting that they may be atypical effectors similar to IRSp53. This raises an interesting question that our data does address however, and that is how "inactive" Rab35, bound to GDP and recruited by IRSp53 and maintained by FIP1 might then be activated, to then recruit its downstream effectors like MICAL1 and OCRL to regulate actin levels in the ICB.

Furthermore, while we could detect binding between either the C2 domain or the RBD domain of FIP1 with Rab35 in cells, we could only confirm direct binding between Rab35:RBD using in vitro experiments, suggesting that either the C2 domain binding is indirect, or that the binding requires something not recapitulated by our in vitro system, such as cellular or lipidic environment or post-translational modifications, for example. This would require further study into the precise function of the FIP1 C2 domain in this context. One such function could be that FIP1 tethers together different vesicles, in a similar manner to the Rab5 effector Rabenosyn-5 which links Rab4 and Rab5 positive vesicles (de Renzis et al., 2002). Our results indicate that in cells, FIP1 can possibly bind Rab35 with its C2 and bind to several different Rabs including Rab11, Rab14, Rab35 with its RBD. It is possible that tethering Rab35 to Rab11 vesicles may have a function in other cellular contexts, similarly to the function of Rabenosyn-5. However, as we could not observe any Rab11 in our Rab35 pulldowns (Fig. 3D), this might only occur for discrete short-lived interactions. These interactions would most likely be dispensable for FIP1 cytokinetic function, as our results clearly indicate that the RBD of FIP1 is dispensable for this

function. In other words, FIP1 function in cytokinesis is Rab11-independent, similarly to what we observed for Rip11 (Laflamme et al., 2017).

Importantly, our results indicate that the C2 domain can dimerize with full-length FIP1 (Fig S2B). This could be the means by which FIP1 maintains Rab35 at the intercellular bridge. Indeed, in this case, FIP1 might act as a scaffold rather than a traditional effector per se. Furthermore, this does not exclude the possibility that FIP1 C2 domain might homodimerize or heterodimerize with other FIP C2 domains such as that of FIP2 or FIP5. These interactions might be important for specific cellular functions, but as neither FIP2 nor FIP5 depletion induced a cytokinesis phenotype, this was not pursued.

In conclusion, this work has led to the identification of a new function for the class I FIPs in cytokinesis and that this function is independent of Rab11 binding. We have also shown that this function is implicated in the Rab35/OCRL/MICAL1 axis involved in regulating actin levels at the ICB prior to abscission in both 2D and 3D cultures (Fig. S4D). These results will be an important stepping stone for further study into the various mechanisms that lead to abscission, and this will have far reaching implications, as cell division regulates virtually all cellular processes.

Materials and Methods

Cell culture and transfections

U2OS, HEK293T, HCT116, HeLa, A375, A549 and MCF7 cells were maintained in 5% CO2 and 37°C in Dulbecco's Modified Eagle's Medium (Life Technology Gibco) supplemented with 10% Fetal Bovine Serum (Wisent), 100 µg/ml Streptomycin (Life Technologies) and 100U/ml of Penicillin (Life Technologies). Transfex (ATCC) was used following manufacturer's instructions for transfecting U2OS cells for exogenous expression, while Polyethylenimine (Polysciences Inc. #23966-1) was used to transfect HEK293T cells for immunoprecipitation experiments. Cells were routinely verified for mycoplasma contamination. As for stable cells lines, U2OS cells were transfected with exogenous constructs and selected using 100 µg/ml of Hygromycin B or 700 µg/ml of G418 depending on the backbone resistance of the plasmid. 7 days post selection, resistant cells were sorted using FACS analysis to produce a heterogeneous population of cells expressing low to medium expression of the different constructs. Cells were then maintained in

selection medium for at least 14 days prior to any experiment being performed to ensure stable integration of the constructs into the genome. For Latrunculin A treatment, following 72h of protein depletion by siRNA, cells were plated for immunofluorescence similarly to other experiments but 8 nM of Latrunculin A was added into the media. Cells were fixed 24h after plating and cell binucleation was assayed similarly to other experiments.

Plasmids

pCDNA3.1-pEGFP-C1-Rab11FIP1A, pCDNA3.1-pEGFP-C1-Rab11FIP1B and pCDNA3.1-pEGFP-C1-Rab11FIP1C were gracious gifts from James Goldenring. pCDNA3.1-pEGFP-C1-empty was produced by removing the Rab11FIP1 insert by PCR linearization of the pCDNA3.1-pEGFP-C1-Rab11FIP1B plasmid and then closing the plasmid by using the KLD enzyme kit (NEB #M0554) following manufacturer's instructions. The pCDNA3.1-mCherry-Rab35 plasmid was produced by first amplifying Rab35 from a U2OS cDNA preparation using the two primers: 5' ATCGGGTACCATGGCCCGGGACTACGACCAC 3' and 5' ATCGTCTAGATTAGCAGCAGCGTTTCTTTCG 3', and this was then cloned into the pCDNA3.1-mCherry-empty vector using KpnI and XbaI restriction enzyme sites which was a gracious gift from Marc Therrien. The N-terminal deletion constructs of Rab11FIP1 were produced using the Q5 polymerase (NEB #M0491) deletion strategy coupled to the KLD reaction kit for the closing of the plasmid. Specifically, the primer 5' GGTGACGATAACAAGGGCG 3' was used in conjunction with either 5' CAGCTCTCCGAATCTTCC 3' (to produce 380-1283), 5' GATTCTCTGATGGGCAGG 3' (to produce 669-1283), 5' ACTCAGTATCAGAGCAAAG 3' (to produce 920-1283), 5' AGACTTCATCCTGTGAAG 3' (to produce 1175-1283) or 5' AAGAAATACAGCCCCTCG 3' (to produce 1211-1283). As for deletion constructs 1-208, primer pair 5' TAAAAGGGCGAATTCTGC 3' was used with 5'AACCACAGACTCATCATC 3' and the plasmid was again closed with the KLD enzyme kit. As for deletion construct 108-1211, primer set 5' GGTGACGATAACAAGGGCG 3' and 5' GAGGTGGACCTGCGGGAT 3' were used to produce 108-1283. This plasmid was then used with primer set 5' CATCATGACCTCATTGTTCAAGTTC 3' with 5' TAAAAGGGCGAATTCTGC 3' to produce 108-1211. Again, linear plasmid was closed using the KLD enzyme kit. For deletion construct 1-1211, the same primer set used to produce 108-1211 were used on the full length

Rab11FIP1B plasmid. Finally, the three mutant constructs Y1254S, I1255E and D1256N were produced using the following primer pairs respectively : 5' GCTGGAAGACtccATTGACAACCTGC 3' --- 5' TCGCGGACCTGGAACTCC 3', 5' GGAAGACTACgaaGACAACCTGCTTGTCAGGGTC 3' --- 5' AGCTCGCGGACCTGGAAC 3' and 5' AGACTACATTaacAACCTGCTTGTCAGGG 3' --- 5' TCCAGCTCGCGGACCTGG 3'. For mApple constructs, mApple-Farnesyl-5 was obtained as a gift from Michael Davidson (Addgene plasmid # 54899 ; RRID:Addgene_54899). This plasmid was first linearized using the primer pair: 5' AATTCTGCAGTCGACGGTACC 3' and 5' CGAAGCTTGAGCTCGAGATC 3'. Next the three Rab11FIPs, FIP1A, FIP1B and FIP1C were respectively amplified using the primer pairs 5' gatctcgagctcaagcttcgATGGGCAGGACCCGTGAG 3' --- 5' gtaccgtcgactgcagaattTTACATCTTTCCTGCTTTTTTGCCAAC 3' (FIP1A), 5' gatctcgagctcaagcttcgATGTCCCTAATGGTCTCG 3' --- 5' gtaccgtcgactgcagaattTTACATCTTTCCTGCTTTTTTG 3' (FIP1B) and 5' gatctcgagctcaagcttcgATGTCCCTAATGGTCTCG 3' --- 5' gtaccgtcgactgcagaattTTACATCTTTCCTGCTTTTTTG 3' (FIP1C). These fragments, along with the linearized mApple plasmid were assembled using Gibson assembly (NEB #E2611), following the manufacturer's instructions. For bacterial plasmids, pET28a and pGEX-6p1 were obtained from the Benjamin Kwok lab and digested with EcoRI/XhoI to linearize them. Then, Rab11FIP1B C2 domain and RBD domain were amplified with the respective primers 5' ATCGGAATTCATGTCCCTAATGGTCTCG 3' --- 5' ATCGCTCGAGTAAACCACAGACTCATCA (C2 domain), 5' ATCGGAATTCAAGAAATACAGCCCCTCG 3' --- 5' ATCGCTCGAGTTACATCTTTCCTGCTTT (RBD domain). These two fragments were digested with EcoRI/XhoI and assembled into the pET28a plasmid using a standard ligation protocol. Rab35WT was amplified using the following primer set 5' ATCGGAATTCATGGCCCGGGACTACGAC 3' --- 5' ATCGCTCGAGTTAGCAGCAGCGTTTCTT 3'. This was then digested with EcoRI/XhoI and assembled into pGEX-6P1. p-DEST15(GST)-Rab11A was a gracious gift from the Matt Smith lab. EGFP-Rab1A was a gift from Marci Scidmore (Addgene plasmid # 49467; http://n2t.net/addgene:49467; RRID: Addgene_49467). EGFP-Rab5 was a gift from Marci Scidmore (Addgene plasmid # 49888; http://n2t.net/addgene:49888; RRID:Addgene_49888).

EGFP-Rab6A was a gift from Marci Scidmore (Addgene plasmid # 49469; http://n2t.net/addgene:49469; RRID: Addgene_49469). GFP-RAB10 was a gift from Michael Bassik (Addgene plasmid # 130883; RRID: Addgene 130883). GFP-Rab11 WT was a gift from Richard Pagano (Addgene plasmid # 12674 ; http://n2t.net/addgene:12674 ; RRID:Addgene_12674). EGFP-Rab13 was a gift from Marci Scidmore (Addgene plasmid # 49548; http://n2t.net/addgene:49548; RRID: Addgene_49548). EGFP-Rab35 was a gift from Marci Scidmore (Addgene plasmid # 49552 ; http://n2t.net/addgene:49552 ; RRID:Addgene_49552). All constructs were validated by sequencing.

Antibodies and other staining reagents

Primary antibodies used were as follows : Rab11FIP1 (Sigma Life Science #HPA025960, used at 1/1000), Rab11FIP2 (Sigma Life Science #HPA037726, used at 1/1000), Rab11FIP5 (Sigma Life Science #HPA036407, used at 1/1000), Rab11FIP3 (Proteintech #25843-1-AP, used at 1/100 for IF), Actin (Millipore C4 #MAB1501, used at 1/10000), GFP (Santa Cruz B-2 #sc-9996, used at 1/2000), GAPDH (Santa Cruz FL-335 #sc-25778, used at 1/1000), mCherry for IP (Abcam #ab183628, 1 ug used per IP condition), mCherry for WB (Abcam #ab167453, used at 1/2000), MICAL1 (Proteintech #14818-1-AP, used at 1/100 for IF), Rab35 (Proteintech #11329-2-AP, used at 1/1000), MKLP1 (Abcam #ab168964, used at 1/100 for IF), CHMP4B (Proteintech #13683-1-AP, used at 1/100 for IF), His-probe (Santa Cruz (H-15) #sc-803, used at 1/1000), β-Tubulin (Abcam #ab6046, used at 1/2000), α-Tubulin (Cell Signaling DM1A #3873, used at 1/1000 for IF). Secondary antibodies for western blotting and immunoprecipitation were AffiniPur Goat Anti-Rabbit (H+L) from Jackson Immunoresearch (111-035-144, used at 1/1000), AffiniPur Mouse Anti-Rabbit (Light-Chain Specific) from Jackson Immunoresearch (211-032-171, used at 1/1000), AffiniPur Goat Anti-Mouse (Light-Chain Specific) from Jackson Immunoresearch (115-035-174, used at 1/1000), AffiniPur Goat Anti-Mouse (H+L) from Jackson Immunoresearch (115-035-062, used at 1/1000). Secondary antibodies and other reagents for immunofluorescence were Alexa Fluor 488 Phalloidin (Invitrogen #A12379, used at 1/1000), Alexa Fluor 555 Phalloidin (Invitrogen #A34055, used at 1/1000), Alexa Fluor 647 Phalloidin (Invitrogen #A22287, used at 1/50), Alexa Fluor 488 Goat Anti-Mouse IgG (Invitrogen #A11029, used at 1/1000), Alexa Fluor 488 Goat Anti-Rabbit IgG (Invitrogen #A11008, used at 1/1000), Alexa Fluor 555 Anti-Mouse IgG (Cell Signaling #4499S, used at

1/1000), Alexa Fluor 555 Anti-Rabbit IgG (Cell Signaling #4413S, used at 1/1000), Alexa Fluor 633 Goat Anti-Rabbit IgG (Invitrogen #A31577, used at 1/1000), Alexa Fluor 635 Goat Anti-Mouse IgG (Invitrogen #A31575, used at 1/1000), DAPI was used to stain nuclei at 1 ug/ml. SiR-Tubulin (Cytoskeleton Inc #CY-SC002, used at 100 nM) was used to monitor tubulin polymerization during live cell imaging.

siRNA treatments

Lipofectamine RNAiMax (ThermoFisher #13778100) was used to transfect cells using siRNA. RNAi duplex sequences for siRNA used were as follows: siControl 5' UUCUCCGAACGUGUCACGUdTdT 3' - 5' ACGUGACACGUUCGGAGAAdTdT 3', siFIP1 5' UUAAUUGUAAUCAUUAACCdTdG 3' - 5'GGUUAAUGAUUACAAUUAAdTdT 3', Rab35 5' GCUCACGAAGAACAGUAAA 3' - UUUACUGUUCUUCGUGAGC 3'. siRNA sequences against FIP2, FIP5 and OCRL were obtained from QIAGEN, wherein sequences are proprietary and unknown. However, targeted sequences are as follows: siFIP2 5' CAGGTGGCAATCAATCTCAAT 3', siFIP5 5' CACCATCCAGTTCACGCGCAA 3' and siOCRL 5'CAGCGGGAGGGTCTCATCAAA 3'.

Western blotting and immunoprecipitation

For western blotting, cells were scraped in 50 mM Tris pH 7.5 containing 1% SDS, sonicated at 70% intensity for 1 minute and then boiled for 5 minutes at 95°C. Samples were then quantified using the BCA Protein Assay Kit (Thermo Scientific Pierce^{TM} #23225). Samples were then mixed with 5X SDS sample loading buffer and loaded onto SDS-PAGE gels (7-15%) to separate proteins according to their molecular weight. Proteins were then transferred onto nitrocellulose and blotted using indicated antibodies following standard laboratory procedures. As for immunoprecipitations, cells were scraped in PBS, and spun down to form a pellet. Pellets were kept at -80°C until used. Pellets were then lysed in lysis buffer containing 50 mM Tris pH 7.5, 5 mM EDTA, 1% Triton X-100 and 150 mM NaCl supplemented with protease inhibitor cocktail (Roche cOmplete #11697498001), 2 mM Imidazole (BioShop #IMD508), 1 mM Sodium Fluoride (Sigma Life Science #S6776), 6 mM Sodium Molybdate (Sigma-Aldrich (M1651), 10 mM Sodium Tartrate (Sigma-Aldrich S4797), 1.2 mM β-glycerophosphate (Sigma-Aldrich #G5422), 1 mM Sodium orthovanadate (Sigma-Aldrich #S6508) and 100 nM Sodium

Pyrophosphate (Sigma-Aldrich #221368) to inhibit all proteases and phosphatases. Lysis occurred for 15 minutes on ice before samples were spun down at 15 000 rpm for 15 minutes. Supernatants were then quantified using the Bradford Reagent (Bio-Rad Protein Assay Dye #5000006). Next, between 1-2 mg of total protein from each sample was incubated overnight with 1 µg of primary antibody and pre-blocked Protein A/G-PLUS Agarose beads (Santa-Cruz #sc-2003). The following morning, the beads were washed five times using lysis buffer and then SDS sample buffer was added with boiling to detach proteins from the beads. IP samples were then loaded on SDS-PAGE gels similarly to above.

Immunofluorescence

Cells plated for immunofluorescence were left to adhere onto coverslips overnight and fixed using 4% PFA. Slides were then washed twice using IF wash buffer composed of PBS supplemented with 0.1% Triton X-100. Slides were then incubated for 1 hour at room temperature in IF blocking buffer composed of PBS, 0.3% Triton X-100, 5% BSA passed through a 0.22 µm filter. Next, the slides were incubated in primary antibodies overnight, all of which were mixed in IF blocking buffer. Slides were then washed three times 5 minutes each using IF wash buffer and then incubated with secondary antibodies for two hours at room temperature. Finally, slides were again washed three times 5 minutes before mounting in VectaShield (Vector Laboratories Canada Inc. #H-1000) and sealed using nail polish. Immunofluorescence was observed using an inverted confocal LSM880 microscope from Zeiss using either a 20x, Plan Apo, NA 0.8, DICII objective for binucleation measurements, a 40X, EC PlnN, NA 1.3, DIC III for Phalloidin staining and MICAL1 enrichment measurements or a 63X, Plan-Apo, NA 1.4 DIC objective for MKLP1, RhoA, FIP3, CHMP4B recruitment..

GST-Pulldown assay

Bacterial protein production

DH5α bacteria containing plasmids coding for His-C2, His-RBD, GST-, GST-Rab11 and GST-Rab35 WT were inoculated into 50 mL cultures with antibiotics overnight. The following morning, the 50 mL cultures were diluted into 500 mL cultures containing antibiotics and 1 mM of isopropyl-β-D-thiogalactoside (IPTG, Bioshop #IPT001) for 8 hours. Cultures were then spun down to pellets and two different lysis were performed. For His-tagged proteins, bacteria were

lysed for 15 minutes on ice in Ni-NTA Lysis buffer composed of 50 mM NaH_2PO_4 (Bioshop #SPM306), 300 mM NaCl, 10 mM Imidazole (BioShop #IMD508), pH 8.0. Next, 1 mg/ml of lysozome (Bioshop #LYS702) was added to the lysis for another 30 minutes on ice. Samples were then sonicated for six 10 second bursts at 100% intensity, allowing for 10 seconds of cooling period between each burst. Samples were then centrifuged at 3750 rpm for 1 hour at 4°C to pellet debris and the supernatant was then filtered through a 0.44um filter. Supernatants were then incubated with 1 mL of Ni-NTA resin (Qiagen #1018244) overnight at 4°C. The following day, beads were washed with Ni-NTA wash buffer composed of Ni-NTA Lysis buffer but containing 20 mM of Imidazole (BioShop #IMD508), a total of 5 times with 5 mL of wash buffer. Proteins were then eluted using Ni-NTA elution buffer composed of Ni-NTA Lysis buffer but containing 250 mM Imidazole. The elutions were kept at -80°C until ready to be used. For the GST protein production, bacterial pellets were resuspended in GST Lysis buffer containing 1 mM Dithiothreitol (DTT), 1 mM Phenylmethylsulfonyl Fluoride (PMSF), 1 mM EDTA and 0.2% Triton X-100 in PBS pH 7.5. To this 1 mg/ml of lysozyme (Bioshop #LYS702) was added followed by vigorous shaking and the samples were left on ice for 60 minutes with occasional shaking. Samples were sonicated similarly to His-tagged proteins. Samples were then centrifuged at 3750 rpm for 1 hour at 4°C and supernatants were then filtered through a 0.44 µm filter. Samples were then rotated overnight at 4°C with 1 mL of Gluthatione resin (GenScript #L00206). The following morning, beads were washed 5 times with PBS and beads were kept as a 20% slurry at 4°C until used.

In vitro nucleotide loading

Guanosine 5′-[β,γ-imido]triphosphate (Sigma #G0635) and Guanosine 5′-[β-thio]diphosphate (Sigma #G7637) 100X solutions (20 mM and 100 mM respectively) were prepared in distilled water. 1X solutions were then incubated with 5 ug of GST-Rab11 or GST-Rab35 beads for 1 hour at 37°C in loading buffer composed of 25 mM Tris pH 7.5, 100 mM NaCl, 10 mM EDTA, 5 mM $MgCl_2$ and 1 mM DTT. The loading reaction was then halted by the addition of 20 mM $MgCl_2$.

GST-Pulldown assay

Either purified proteins (for His-tags) or beads (GST-proteins) were loaded on SDS-PAGE gels beside a BSA ladder to quantify samples. Using these measurements, 5 ug of His-C2 or His-RBD were incubated overnight at 4°C with 5 ug of either GST-, GST-Rab11 or GST-Rab35 (either empty, loaded with GTP or loaded with GDP and completed to the same bead bed using empty glutathione agarose beads) in IVB buffer composed of 50 mM Tris pH 7.5, 100 mM NaCl, 10 mM MgCl2, 0.1% Triton X-100 and 0.05% BSA. The following day, beads were washed using IVB buffer 5 times and then proteins were eluted using SDS sample loading buffer. Proteins were then loaded on SDS-PAGE gels and proteins were either revealed using Coomassie Brilliant Blue Staining.

3D cultures

For 3D cultures, a thin layer of GelTrex (Gibco #A14132-02) was spread out into the bottom of an Ibidi 8 well chamber slide (Ibidi #80826) and left to solidify in the cell culture incubator at 5% CO2 and 37°C for 15 minutes. Next, cells were trypsinized and 10 000 cells of an individualized cell solution in DMEM supplemented with 2% GelTrex was layered on the solidified basal layer. Media was delicately removed and changed every 3 days for a total of 10 days before cells were fixed using 4% PFA and whole wells were treated for immunofluorescence similarly to cells on slides.

Live-imaging

Cells plated for live-imaging were first counted and 10 000 cells were plated similarly to other cell lines explained above into Ibidi 8 well chamber slides (Ibidi #80826) in the presence of 100 nmol of SiR-Tubulin (Cytoskeleton Inc #CY-SC002) for 24 hours prior to imaging to avoid altering microtubule dynamics. Slides were then mounted into an LSM700 live-cell imaging mount on the inverted LSM700 confocal microscope (Zeiss) to maintain 5% CO2 and 37°C during movie acquisitions. Cells were filmed using either a 20x, Plan Apo, NA 0.8, DICII objective or a 40x, Plan Apo, NA 1.4 DIC objective and movies were acquired using the Zen software.

Fluorescence intensity measurements

For fluorescence intensity measurements, individual frames of live-imaging movies were first sequentially opened in ImageJ as a stacked image. Next, for different measurements, the custom region function was used to draw a custom region of interest (ROI), which either followed the cell-cell interface or the entire Sir-Tubulin stained mitotic spindle in the far-red channel. These regions were then measured for average fluorescence signal in the appropriate green and red channels and a measurement of the average fluorescence intensity of the entire cell was also used to normalize the enrichment signals. This was then repeated for every time point over the course of the movie and graphs of the averages were produced using Prism Graphpad software. Dark lines represent the average signal while the shaded areas represent the S.E.M overtime. Two-tailed Student T-test was then used for each point to compare significance.

Statistical analyses

Paired and unpaired Two-tailed Student t-tests and Mann-Whitney tests were performed using the Prism Graphpad. Values are expressed as means ± standard errors of the means (SEM) or means ± standard deviations (SD), as indicated in the figure legends. p-values are noted on respective figures, wherein p-value < 0.05 = *, p-value < 0.01 = **, p-value < 0.001 = ***, p-value < 0.0001 = ****. Tests were done on at least three independent experiments and then all individual points were pooled together to produce figures unless data specifically shows means.

Acknowledgements

NVGI designed and performed all experiments and drafted the manuscript. GE supervised all work and participated in drafting manuscript. We would like to thank Giorgio Scita (University of Milan) for his input on the manuscript. Next, we would like to thank the Goldenring lab (Vanderbilt University Medical Center) for the pEGFP-FIP1A, pEGFP-FIP1B and pEGFP-FIP1C plasmids, the Smith lab (IRIC, Université de Montréal) for the p-DEST15(GST)-Rab11A plasmid, the Echard lab (Institut Pasteur) for the siRNA targeting Rab35, the Piekny lab (University of Concordia) for the pEGFP-RhoA-binding-domain-of-anillin plasmid, the Therrien lab (IRIC, Université de Montréal) for the pCDNA3.1-mCherry-empty plasmid as well as the 293T, HCT116, A375, A549, MCF7 and Caco-2 cell lines, the Borden lab (IRIC, Université de Montréal) for the U2OS cell line and the Meloche lab (IRIC Université de Montréal) for the

HeLa cell line. We would also like to thank Christian Charbonneau from the core Microscopy platform for assistance in all microscopy experiments as well as the FACS platform (IRIC, Université de Montréal) for the FACS cell sorting experiments.

Funding

This work was supported by the Canadian Institutes of Health Research operating grant [MOP-148560]; and a discovery grant from the Natural Sciences and Engineering Research Council of Canada. NVGI received an Institut de recherche en immunologie et en cancérologie PhD scholarship as well as a PhD funding scholarship from Fonds de recherche du Québec – Nature et technologies.

References

Ai, E. & Skop, A. R. (2009). Endosomal recycling regulation during cytokinesis. *Commun Integr Biol,* **2,** 444-7.

Baetz, N. W. & Goldenring, J. R. (2013). Rab11-family interacting proteins define spatially and temporally distinct regions within the dynamic Rab11a-dependent recycling system. *Mol Biol Cell,* **24,** 643-58.

Ben El Kadhi, K., Emery, G. & Carreno, S. (2012). The unexpected role of Drosophila OCRL during cytokinesis. *Commun Integr Biol,* **5,** 291-3.

Bisi, S., Marchesi, S., Rizvi, A., Carra, D., Beznoussenko, G. V., Ferrara, I., Deflorian, G., Mironov, A., Bertalot, G., Pisati, F., et al. (2020). IRSp53 controls plasma membrane shape and polarized transport at the nascent lumen in epithelial tubules. *Nature Communications,* **11,** 3516.

Bökenkamp, A. & Ludwig, M. (2016). The oculocerebrorenal syndrome of Lowe: an update. *Pediatr Nephrol,* **31,** 2201-2212.

Bruno, J., Brumfield, A., Chaudhary, N., Iaea, D. & Mcgraw, T. E. (2016). SEC16A is a RAB10 effector required for insulin-stimulated GLUT4 trafficking in adipocytes. *J Cell Biol,* **214,** 61-76.

Carim, S. C., Ben El Kadhi, K., Yan, G., Sweeney, S. T., Hickson, G. R., Carreno, S. & Lowe, M. (2019a). IPIP27 Coordinates PtdIns(4,5)P2 Homeostasis for Successful Cytokinesis. *Curr Biol,* **29,** 775-789.e7.

Carim, S. C., Ben El Kadhi, K., Yan, G., Sweeney, S. T., Hickson, G. R., Carréno, S. & Lowe, M. (2019b). IPIP27 Coordinates PtdIns(4,5)P(2) Homeostasis for Successful Cytokinesis. *Curr Biol,* **29,** 775-789.e7.

Carson, B. P., Del Bas, J. M., Moreno-Navarrete, J. M., Fernandez-Real, J. M. & Mora, S. (2013). The rab11 effector protein FIP1 regulates adiponectin trafficking and secretion. *PLoS One,* **8,** e74687.

Cauvin, C., Rosendale, M., Gupta-Rossi, N., Rocancourt, M., Larraufie, P., Salomon, R., Perrais, D. & Echard, A. (2016). Rab35 GTPase Triggers Switch-like Recruitment of the Lowe Syndrome Lipid Phosphatase OCRL on Newborn Endosomes. *Curr Biol,* **26,** 120-8.

Chesneau, L., Dambournet, D., Machicoane, M., Kouranti, I., Fukuda, M., Goud, B. & Echard, A. (2012). An ARF6/Rab35 GTPase cascade for endocytic recycling and successful cytokinesis. *Curr Biol,* **22,** 147-53.

Dambournet, D., Machicoane, M., Chesneau, L., Sachse, M., Rocancourt, M., El Marjou, A., Formstecher, E., Salomon, R., Goud, B. & Echard, A. (2011). Rab35 GTPase and OCRL phosphatase remodel lipids and F-actin for successful cytokinesis. *Nat Cell Biol,* **13,** 981-8.

De Renzis, S., Sönnichsen, B. & Zerial, M. (2002). Divalent Rab effectors regulate the sub-compartmental organization and sorting of early endosomes. *Nat Cell Biol,* **4,** 124-33.

Echard, A. (2008). Membrane traffic and polarization of lipid domains during cytokinesis. *Biochem Soc Trans,* **36,** 395-9.

Erneux, C., Ghosh, S., Ramos, A. R. & Edimo, W. E. (2016). New Functions of the Inositol Polyphosphate 5-Phosphatases in Cancer. *Curr Pharm Des,* **22,** 2309-14.

Eva, R., Dassie, E., Caswell, P. T., Dick, G., Ffrench-Constant, C., Norman, J. C. & Fawcett, J. W. (2010). Rab11 and its effector Rab coupling protein contribute to the trafficking of beta 1 integrins during axon growth in adult dorsal root ganglion neurons and PC12 cells. *J Neurosci,* **30,** 11654-69.

Fan, G. H., Lapierre, L. A., Goldenring, J. R. & Richmond, A. (2003). Differential regulation of CXCR2 trafficking by Rab GTPases. *Blood,* **101,** 2115-24.

Fan, G. H., Lapierre, L. A., Goldenring, J. R., Sai, J. & Richmond, A. (2004). Rab11-family interacting protein 2 and myosin Vb are required for CXCR2 recycling and receptor-mediated chemotaxis. *Mol Biol Cell,* **15,** 2456-69.

Festa, B. P., Berquez, M., Gassama, A., Amrein, I., Ismail, H. M., Samardzija, M., Staiano, L., Luciani, A., Grimm, C., Nussbaum, R. L., et al. (2019). OCRL deficiency impairs endolysosomal function in a humanized mouse model for Lowe syndrome and Dent disease. *Hum Mol Genet,* **28,** 1931-1946.

Frémont, S. & Echard, A. (2018). Membrane Traffic in the Late Steps of Cytokinesis. *Current Biology,* **28,** R458-R470.

Frémont, S., Hammich, H., Bai, J., Wioland, H., Klinkert, K., Rocancourt, M., Kikuti, C., Stroebel, D., Romet-Lemonne, G., Pylypenko, O., et al. (2017). Oxidation of F-actin controls the terminal steps of cytokinesis. *Nat Commun,* **8,** 14528.

Gatta, A. T. & Carlton, J. G. (2019). The ESCRT-machinery: closing holes and expanding roles. *Curr Opin Cell Biol,* **59,** 121-132.

Holder, J., Poser, E. & Barr, F. A. (2019). Getting out of mitosis: spatial and temporal control of mitotic exit and cytokinesis by PP1 and PP2A. *FEBS Letters,* **593,** 2908-2924.

Hwang, M. H., Cho, K. H., Jeong, K. J., Park, Y. Y., Kim, J. M., Yu, S. L., Park, C. G., Mills, G. B. & Lee, H. Y. (2017). RCP induces Slug expression and cancer cell invasion by stabilizing β1 integrin. *Oncogene,* **36,** 1102-1111.

Jin, M. & Goldenring, J. R. (2006). The Rab11-FIP1/RCP gene codes for multiple protein transcripts related to the plasma membrane recycling system. *Biochim Biophys Acta,* **1759,** 281-95.

Jing, J., Junutula, J. R., Wu, C., Burden, J., Matern, H., Peden, A. A. & Prekeris, R. (2010). FIP1/RCP binding to Golgin-97 regulates retrograde transport from recycling endosomes to the trans-Golgi network. *Mol Biol Cell,* **21,** 3041-53.

Klinkert, K. & Echard, A. (2016). Rab35 GTPase: A Central Regulator of Phosphoinositides and F-actin in Endocytic Recycling and Beyond. *Traffic,* **17,** 1063-77.

Klinkert, K., Rocancourt, M., Houdusse, A. & Echard, A. (2016). Rab35 GTPase couples cell division with initiation of epithelial apico-basal polarity and lumen opening. *Nat Commun,* **7,** 11166.

Kouranti, I., Sachse, M., Arouche, N., Goud, B. & Echard, A. (2006). Rab35 regulates an endocytic recycling pathway essential for the terminal steps of cytokinesis. *Curr Biol,* **16,** 1719-25.

Laflamme, C., Galan, J. A., Ben El Kadhi, K., Méant, A., Zeledon, C., Carréno, S., Roux, P. P. & Emery, G. (2017). Proteomics Screen Identifies Class I Rab11 Family Interacting Proteins as Key Regulators of Cytokinesis. *Mol Cell Biol,* **37**.

Lall, P., Lindsay, A. J., Hanscom, S., Kecman, T., Taglauer, E. S., Mcveigh, U. M., Franklin, E., Mccaffrey, M. W. & Khan, A. R. (2015). Structure-Function Analyses of the Interactions between Rab11 and Rab14 Small GTPases with Their Shared Effector Rab Coupling Protein (RCP). *J Biol Chem,* **290,** 18817-32.

Li, D., Kuehn, E. W. & Prekeris, R. (2014a). Kinesin-2 mediates apical endosome transport during epithelial lumen formation. *Cell Logist,* **4,** e28928.

Li, D., Mangan, A., Cicchini, L., Margolis, B. & Prekeris, R. (2014b). FIP5 phosphorylation during mitosis regulates apical trafficking and lumenogenesis. *EMBO Rep,* **15,** 428-37.

Lindsay, A. J. & Mccaffrey, M. W. (2004). The C2 domains of the class I Rab11 family of interacting proteins target recycling vesicles to the plasma membrane. *J Cell Sci,* **117,** 4365-75.

Lindsay, A. J. & Mccaffrey, M. W. (2005). Purification and functional properties of Rab11-FIP2. *Methods Enzymol,* **403,** 491-9.

Moore, R. H., Millman, E. E., Alpizar-Foster, E., Dai, W. & Knoll, B. J. (2004). Rab11 regulates the recycling and lysosome targeting of beta2-adrenergic receptors. *J Cell Sci,* **117,** 3107-17.

Nalefski, E. A. & Falke, J. J. (1996). The C2 domain calcium-binding motif: structural and functional diversity. *Protein Sci,* **5,** 2375-90.

Nedvetsky, P. I., Stefan, E., Frische, S., Santamaria, K., Wiesner, B., Valenti, G., Hammer, J. A., 3rd, Nielsen, S., Goldenring, J. R., Rosenthal, W., et al. (2007). A Role of myosin Vb and Rab11-FIP2 in the aquaporin-2 shuttle. *Traffic,* **8,** 110-23.

Neto, H., Balmer, G. & Gould, G. (2013). Exocyst proteins in cytokinesis: Regulation by Rab11. *Commun Integr Biol,* **6,** e27635.

Peden, A. A., Schonteich, E., Chun, J., Junutula, J. R., Scheller, R. H. & Prekeris, R. (2004). The RCP-Rab11 complex regulates endocytic protein sorting. *Mol Biol Cell,* **15,** 3530-41.

Peterman, E. & Prekeris, R. (2019). The postmitotic midbody: Regulating polarity, stemness, and proliferation. *J Cell Biol,* **218,** 3903-3911.

Prekeris, R. (2011). Actin regulation during abscission: unexpected roles of Rab35 and endocytic transport. *Cell Res,* **21,** 1283-5.

Qi, M., Williams, J. A., Chu, H., Chen, X., Wang, J. J., Ding, L., Akhirome, E., Wen, X., Lapierre, L. A., Goldenring, J. R., et al. (2013). Rab11-FIP1C and Rab14 direct plasma membrane sorting and particle incorporation of the HIV-1 envelope glycoprotein complex. *PLoS Pathog,* **9,** e1003278.

Rainero, E., Caswell, P. T., Muller, P. A., Grindlay, J., Mccaffrey, M. W., Zhang, Q., Wakelam, M. J., Vousden, K. H., Graziani, A. & Norman, J. C. (2012). Diacylglycerol kinase α controls RCP-dependent integrin trafficking to promote invasive migration. *J Cell Biol,* **196,** 277-95.

Sechi, S., Colotti, G., Belloni, G., Mattei, V., Frappaolo, A., Raffa, G. D., Fuller, M. T. & Giansanti, M. G. (2014). GOLPH3 is essential for contractile ring formation and Rab11 localization to the cleavage site during cytokinesis in Drosophila melanogaster. *PLoS Genet,* **10,** e1004305.

Sugimoto, K., Nishi, H., Miyazawa, T., Fujita, S., Okada, M. & Takemura, T. (2014). A novel OCRL1 mutation in a patient with the mild phenotype of Lowe syndrome. *Tohoku J Exp Med,* **232,** 163-6.

Takahashi, S., Takei, T., Koga, H., Takatsu, H., Shin, H. W. & Nakayama, K. (2011). Distinct roles of Rab11 and Arf6 in the regulation of Rab11-FIP3/arfophilin-1 localization in mitotic cells. *Genes Cells,* **16,** 938-50.

Vicinanza, M., Di Campli, A., Polishchuk, E., Santoro, M., Di Tullio, G., Godi, A., Levtchenko, E., De Leo, M. G., Polishchuk, R., Sandoval, L., et al. (2011). OCRL controls trafficking through early endosomes via PtdIns4,5P(2)-dependent regulation of endosomal actin. *Embo j,* **30,** 4970-85.

Vietri, M., Radulovic, M. & Stenmark, H. (2020). The many functions of ESCRTs. *Nat Rev Mol Cell Biol,* **21,** 25-42.

Willenborg, C., Jing, J., Wu, C., Matern, H., Schaack, J., Burden, J. & Prekeris, R. (2011). Interaction between FIP5 and SNX18 regulates epithelial lumen formation. *J Cell Biol,* **195,** 71-86.

Figures

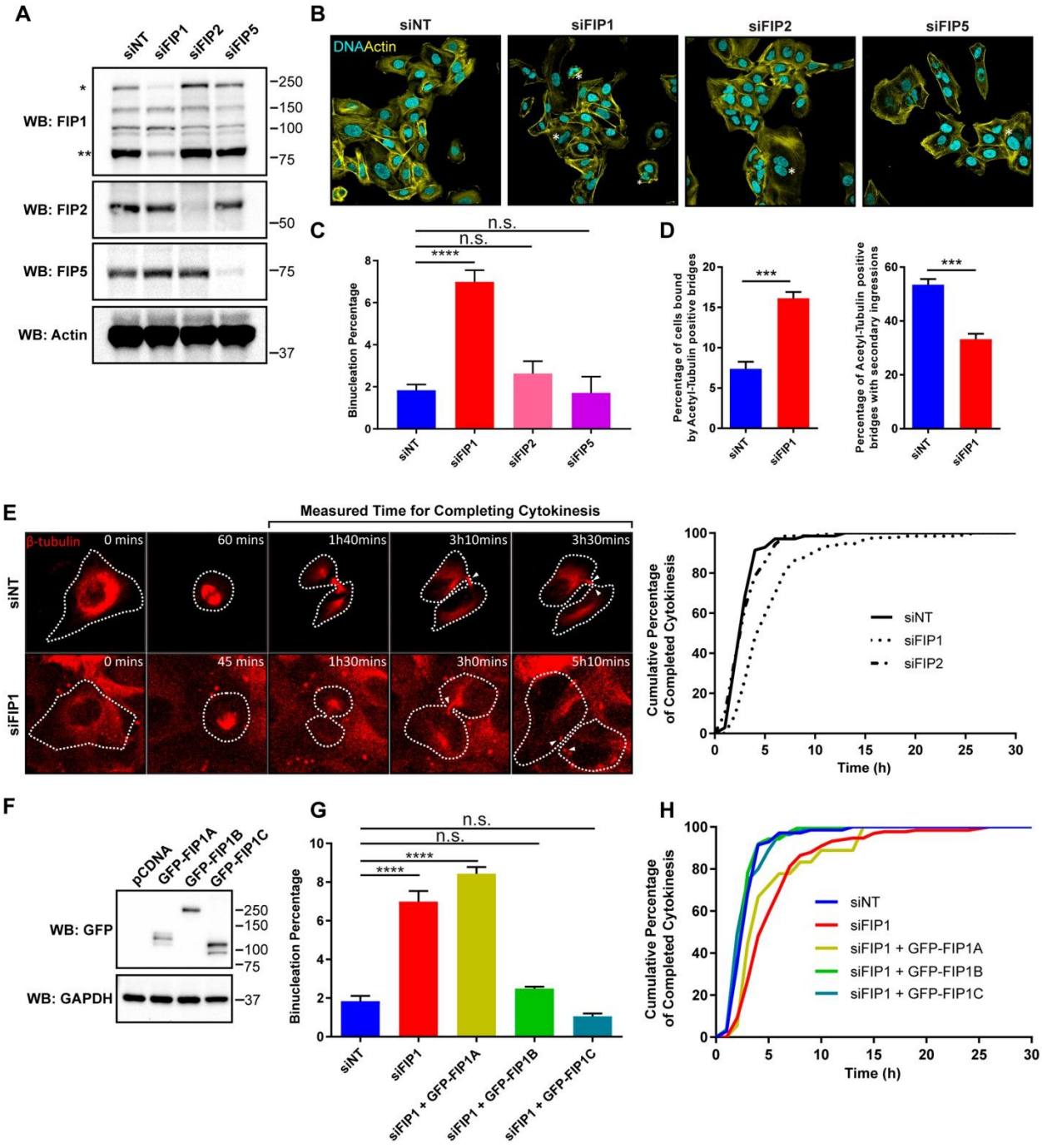

Fig 1: FIP1 is required for timely cytokinesis completion

A) Representative western blot showing indicated protein depletions. Note that FIP1 antibody has non-specific bands and single star denotes FIP1B, double star denotes FIP1C. B) Representative images of cells depleted for FIP1, FIP2, FIP5 stained for Actin (yellow) and

DNA (cyan). Binucleated cells are noted with stars. C) Quantifications of average cellular binucleation. siNT n=496, siFIP1 n=719, siFIP2 n=643, siFIP5 n=107. P-value < 0.0001 = ****, n.s. = not significant, Two-tailed Student T-test. D) (left) Quantifications of percentage of cells bound by acetyl-tubulin-positive intercellular bridges. siNT n=1374, siFIP1 n=1731. P-value < 0.001 = ***. Two-tailed Student T-test. (right) Quantifications of percentage of cells bound by acetyl-tubulin-positive intercellular bridges that show secondary ingressions. siNT n=45, siFIP1 n=53. P-value < 0.001 = ***. Two-tailed Student T-test. E) (left) Representative images of how cytokinesis timing was measured. Timing was measured as the time between the frame of telophase and the frame where the mitotic spindle (indicated by white arrows) was severed. Cells were stained with SiR-Tubulin (red). (right) Quantification of cumulative cytokinesis timing for siNT n=71, siFIP1 n=133 and siFIP2 n=72 overtime. F) Western blot showing expression of exogenous GFP-FIP1A, GFP-FIP1B and GFP-FIP1C constructs in stable cell lines. G) Quantification of average cellular binucleation following rescue experiments. GFP-FIP1A n=509, GFP-FIP1B n=170, GFP-FIP1C n=251. P-value < 0.0001 = ****, n.s. = not significant, Two-tailed Student T-test. H) Quantification of cumulative cytokinesis timing for rescue constructs. GFP-FIP1A n=18, GFP-FIP1B n=19, GFP-FIP1C n=26.

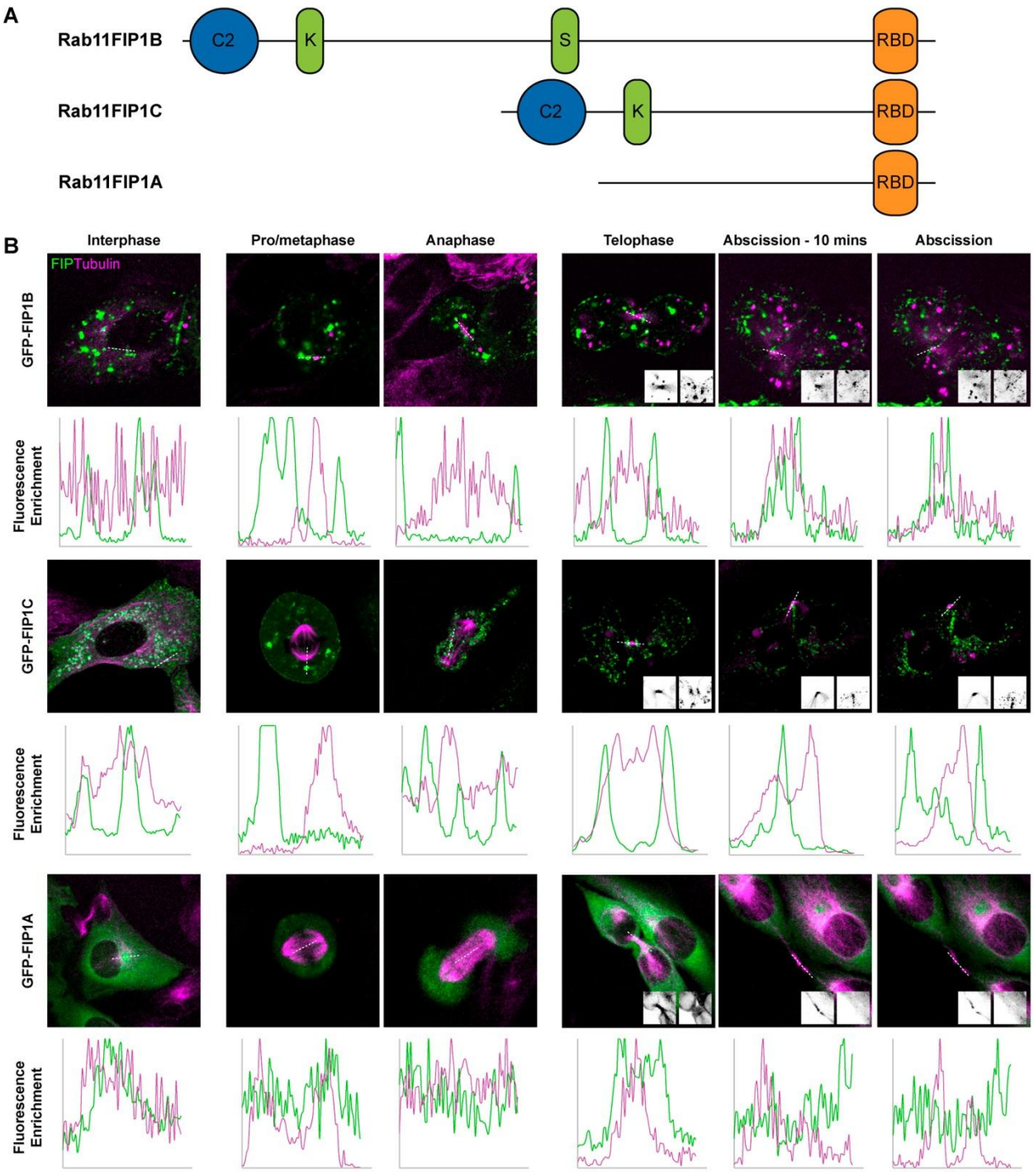

Fig 2: FIP1B and FIP1C localize to the midbody, abscission site and daughter cell:cell interface during mitosis

A) Schematic representation of FIP1 isoforms showing N-terminal C2 domains, lysine rich motif (K), serine-rich motif (S) and C-terminal Rab11-binding domain (RBD). B) Still images of stable cell lines expressing either GFP-FIP1B, GFP-FIP1C or GFP-FIP1A progressing through the phases of mitosis, stained with SiR-Tubulin (magenta) to observe Tubulin and GFP-FIPs in green. Zoomed-in black and white images of the spindle and FIP are in the lower corner of each merge. Line scans were drawn to demonstrate localization of normalized fluorescence intensity through the mitotic spindle as cells progress from telophase to cytokinesis.

A

PROTEIN	SC	SAINT
RAB11A	143	1
STX7	99	1
RHOB	26.5	1
KRAS(Q61H)	26.5	1
RAB9A	21.5	1
RAB35	19	0.98
OCLN	14	0.99
STX6	13	1
ZFPL1	13	0.99
EBAG9	11.5	1
CAV1	11.5	1
MARCKS	12	0.96
LYN	11.5	0.95
LAMP2	11	0.96
RAB4A	10	0.95
FLOT1	9.5	0.94
LCK	9	0.91
CXADR	9	0.93
LAMTOR1	8.5	0.9
LAMP3	8.5	0.92
RAB5A	6	0.9

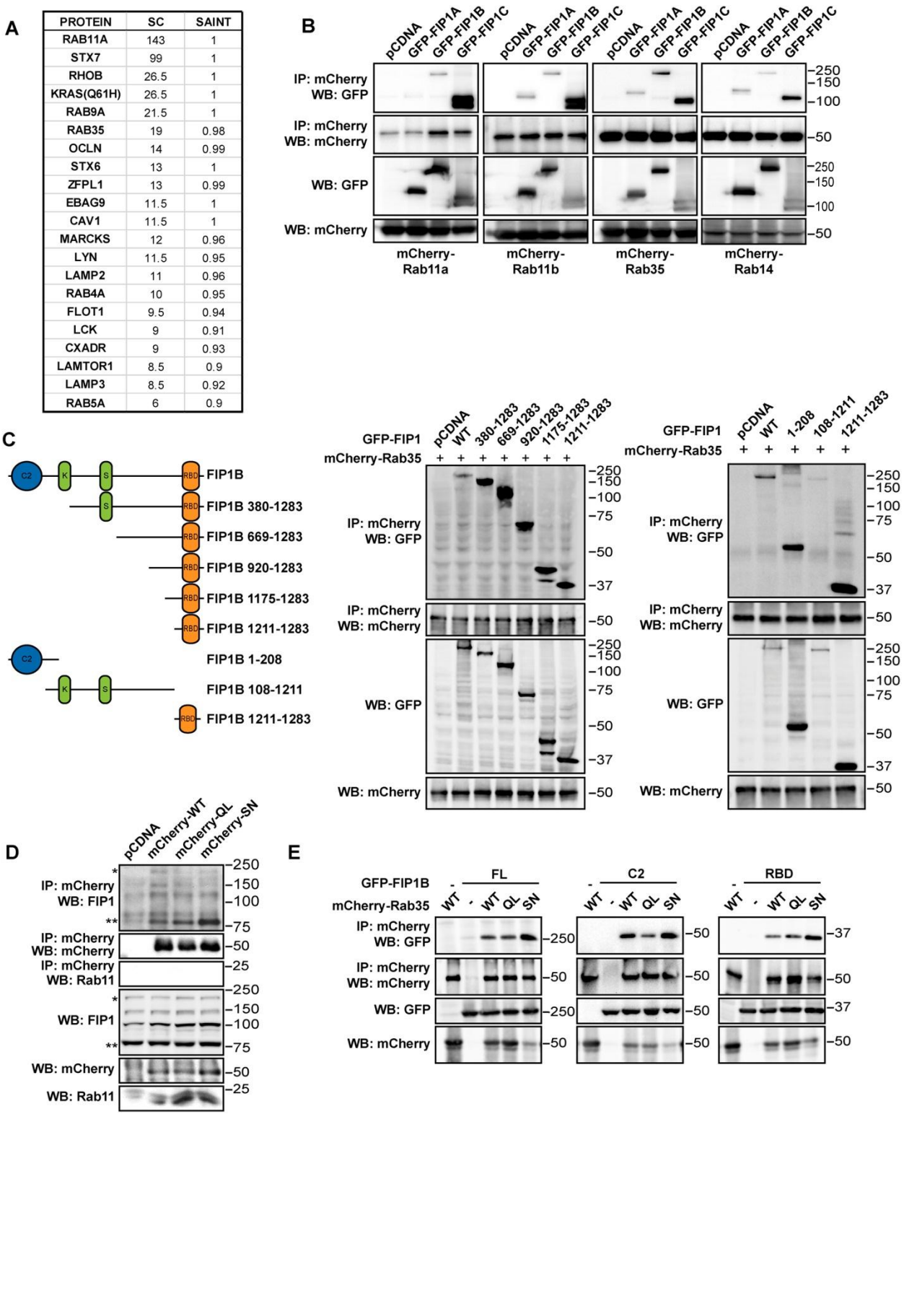

Fig 3: Rab11FIP1 interacts with Rab35 via both its N and C-terminus

A) Summary table of publicly available Bio-ID interactome dataset for FIP1 from https://humancellmap.org, showing average Spectral Counts (SC) and SAINT score for interactors. B) Immunoprecipitation of indicated mCherry-Rabs with exogenous GFP-FIP1 isoforms. C) (left) Schematic representation of FIP1 constructs used for immunoprecipitations used in (right) showing interaction between FIP1 N-terminal deletion constructs with mCherry-Rab35 as well as the interaction between FIP1 N-terminal C2 domain, middle domain and C-terminal RBD domain with mCherry-Rab35. D) Immunoprecipitation of endogenous FIP1 and Rab11 by mCherry-Rab35 wild-type (WT), catalytically active mutant (QL) and dominant negative (SN). Note that FIP1 antibody has non-specific bands and single star denotes FIP1B, double star denotes FIP1C. E) Immunoprecipitation of GFP-FIP1B full length, C2 domain or RBD domain by mCherry-Rab35 wild-type (WT), catalytically active mutant (QL) and dominant negative (SN).

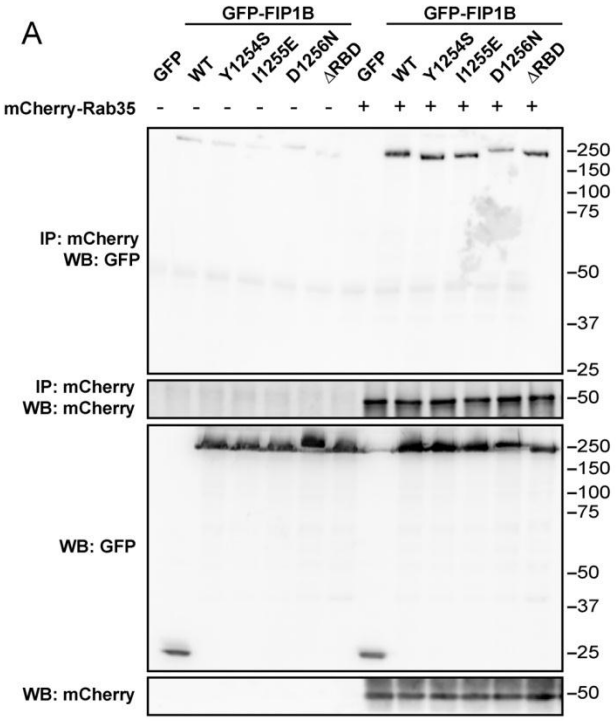

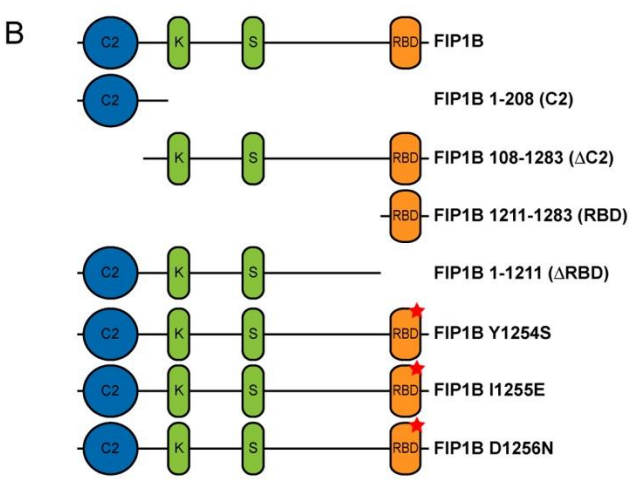

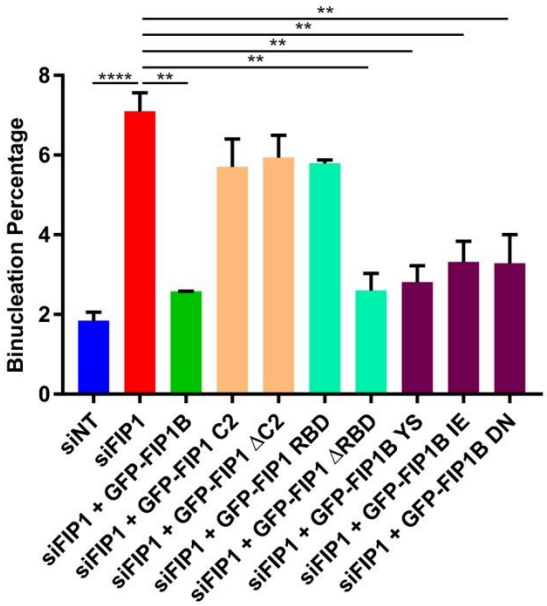

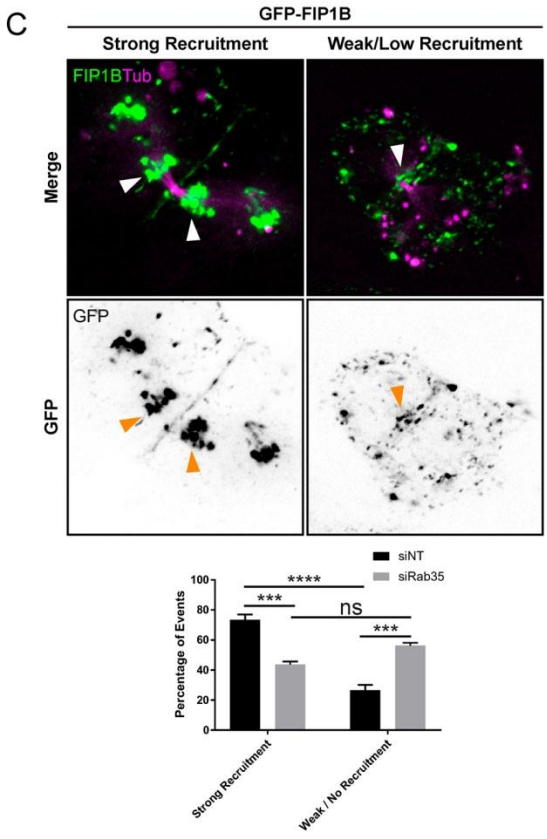

Fig 4: FIP1 binding to Rab35 is required for its proper localization during cytokinetic abscission

A) Immunoprecipitation of GFP-FIP1 RBD mutants by mCherry-Rab35. B) (upper) Schematic representation of FIP1 constructs used for siFIP1 binucleation rescue experiments. (lower) Binucleation percentage of cells either treated with siNT n=504 or siFIP1 n=706 coupled with stable expression of rescue constructs containing different domains of FIP1. (GFP-FIP1B n=173, GFP-FIP1B C2 n=189, GFP-FIP1ΔC2 n=98, GFP-FIP1 RBD n=240, GFP-FIP1ΔRBD n=136, GFP-FIP1B YS n=168, GFP-FIP1B IE n=109, GFP-FIP1B DN n=160). P-value < 0.01 = **, P-value < 0.0001 = ****, Two-tailed Student T-test. C) (upper) Representative images of two categories of GFP-FIP1B recruitment to the intercellular bridge showing either strong, or weak/undetected localization. Inverted black and white images of the green channel (FIP1B) are also shown below. (lower) Quantification of the percentage of occurrence for each category in (upper) following either siNT n=91 or siRab35 n=135 treatment. P-value < 0.001 = ***, P-value < 0.0001 = ****, Two-tailed Student T-test.

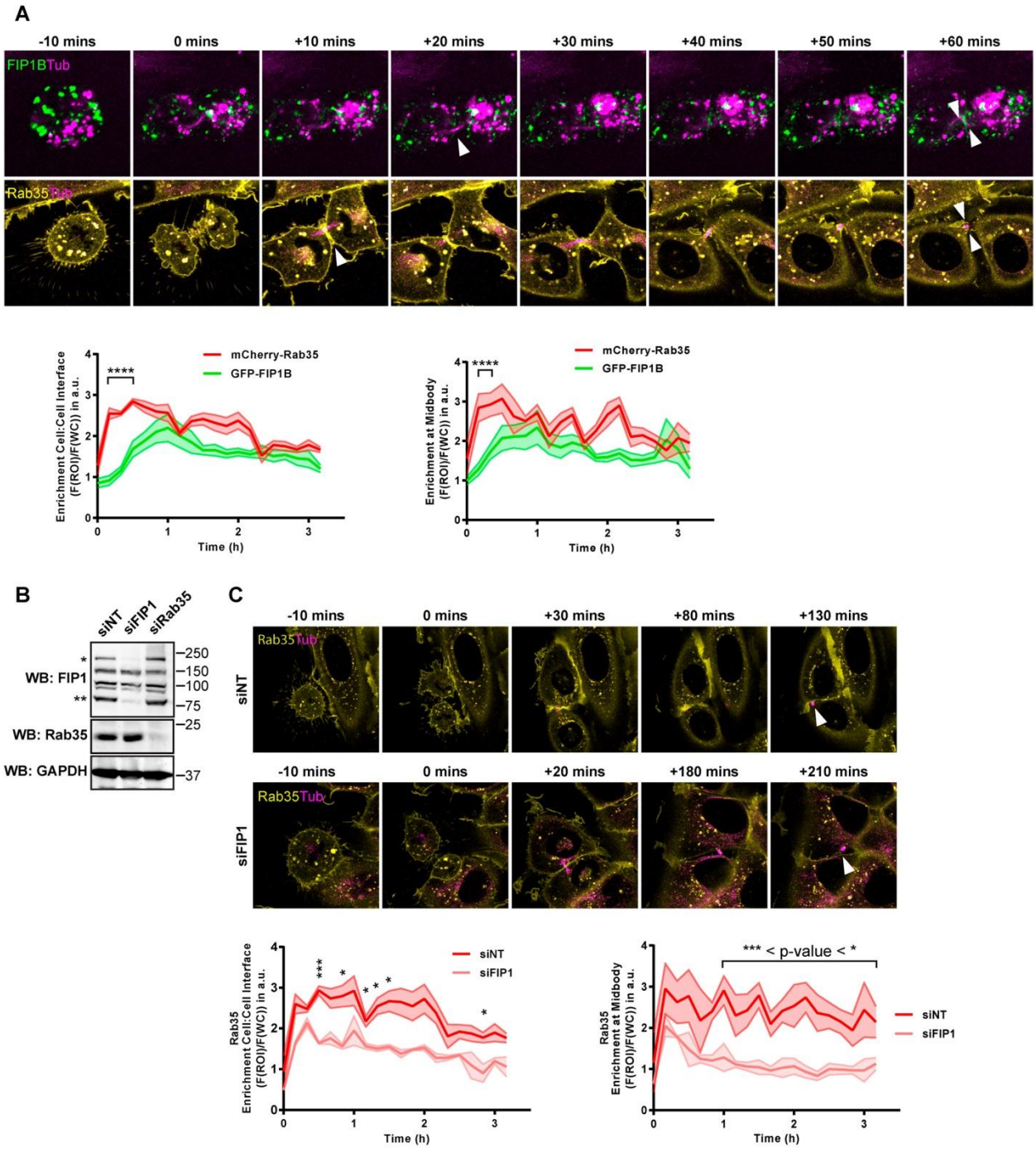

Fig 5: FIP1 is required for maintaining Rab35 at the midbody

A) (upper) Representative images of cells progressing through mitosis that stably express either GFP-FIP1B full length (in green) or mCherry-Rab35 (in yellow). Cells are stained with SiR-Tubulin and tubulin signal is shown in magenta. Time zero is set as the frame corresponding to telophase. Arrows denote the ICB linking daughter cells or the remnants of the spindle after

abscission. (lower left) Normalized average fluorescence intensity of either GFP-FIP1B (in green) or mCherry-Rab35 (in red) overtime at the cell-cell interphase between daughter cells where time point 0 is the first observance of telophase. mCherry-Rab35 n=10, GFP-FIP1B n=18. P-value < 0.0001 = ****, Two-tailed Student T-test. (lower right) Normalized average fluorescence intensity of either GFP-FIP1B (in green) or mCherry-Rab35 (in red) overtime at the midbody where time point 0 is the first observance of telophase. mCherry-Rab35 n=10, GFP-FIP1B n=18. P-value < 0.0001 = ****, Two-tailed Student T-test. B) Representative Western blot showing the depletion of FIP1 or Rab35 in the subsequent experiment. Note that FIP1 antibody has non-specific bands and single star denotes FIP1B, double star denotes FIP1C. C) Representative images of cells progressing through mitosis that stably express mCherry-Rab35 (shown in yellow) that were treated with either siNT or siFIP1. Arrows denote the location of abscission. (lower left) Normalized average fluorescence intensity of mCherry-Rab35 overtime following either siNT or siFIP1 treatment, at the cell-cell interphase between daughter cells where time point 0 is the first observance of telophase. siNT n=10, siFIP1 n=8. P-value < 0.0001 = ****, P-value < 0.05 = *, Two-tailed Student T-test. (lower right) Normalized average fluorescence intensity of mCherry-Rab35 overtime following either siNT or siFIP1 treatment, at the midbody where time point 0 is the first observance of telophase. siNT n=10, siFIP1 n=8. P-value < 0.05 = *, P-value < 0.001 = ***, Two-tailed Student T-test.

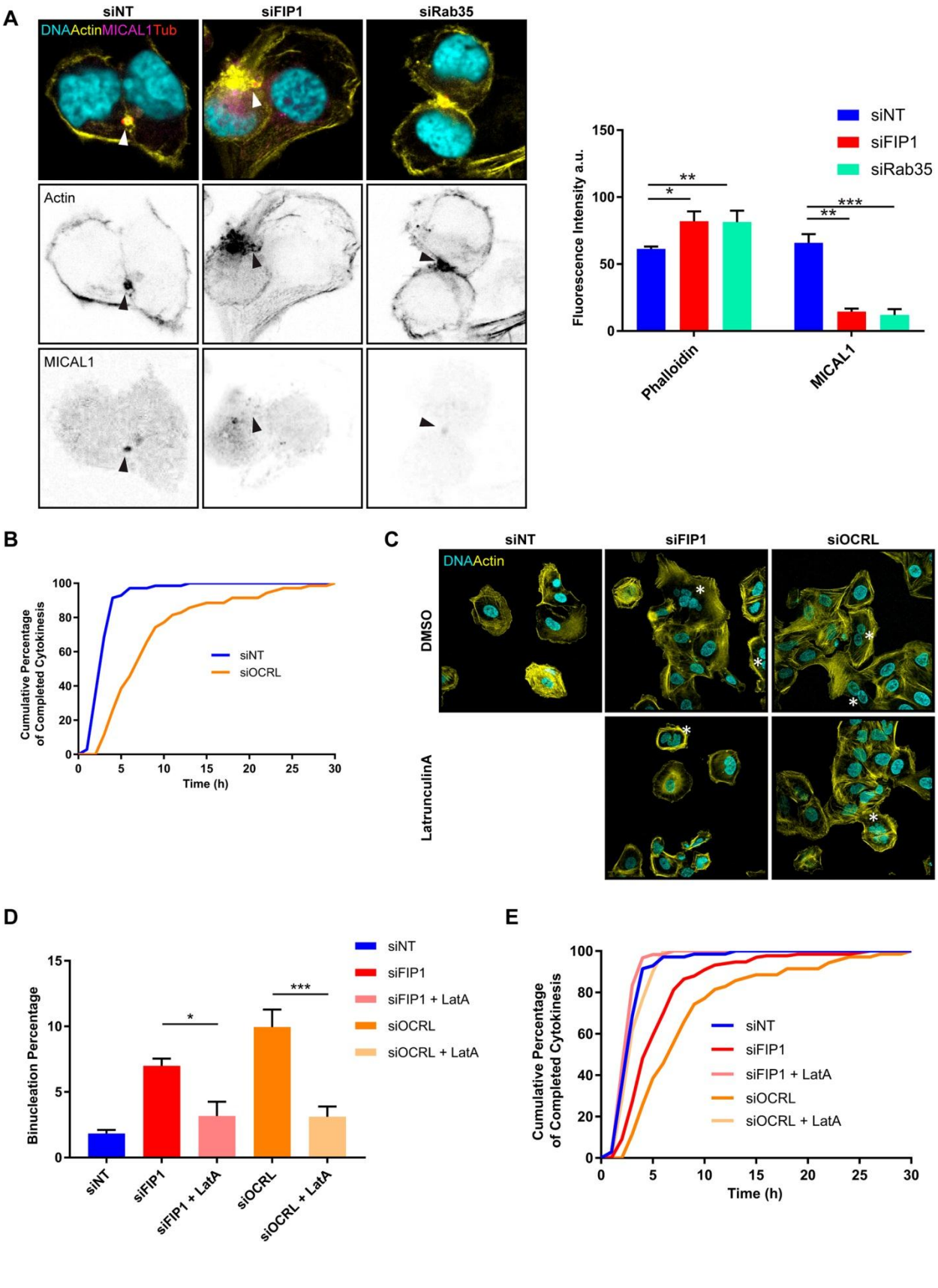

Fig 6: FIP1 maintenance of Rab35 and its effectors OCRL and MICAL1 at the midbody is required for curbing actin overaccumulation and cytokinesis defects

A) (left) Representative images of cells treated with either siNT, siFIP1 or siRab35 wherein DNA is stained in cyan, actin in yellow, MICAL1 in magenta and β-Tubulin in red. Inverted black and white images of the yellow channel of actin and magenta channel of MICAL1 are shown below. Arrows indicate either the accumulation of actin at the intercellular bridge or the localization of MICAL1 in the midbody. (right) Quantification of either actin or MICAL1 average normalized fluorescence intensity signal in a ROI around the ICB, measured as the region of the β-Tubulin staining and surrounding area in siNT n=12, siFIP1 n=11 or siRab35 n=13 conditions. Fluorescence intensity was measured as the fluorescence intensity minus that of the background signal. P-value < 0.05 = *, P-value < 0.01 = **, P-value < 0.001 = ***, Two-tailed Student T-test. B) Cumulative percentage of cells having completed cytokinesis for cells depleted of OCRL. C) Representative immunofluorescence of cells treated with either siNT, siFIP1 or siOCRL followed by treatment with either DMSO or Latrunculin A. Binucleated cells are indicated with white stars. D) Binucleation percentage of cells treated with siNT n=504 siFIP1 n=766 or OCRL n=522 and subsequently treated with Latrunculin A (siFIP1 n=300, siOCRL n=300) as indicated in the materials and methods section. P-value < 0.05 = *, P-value < 0.001 = ***, Two-tailed Student T-test. E) Cumulative cytokinesis timing for siNT n=70, siFIP1 n=133 and siOCRL n=70 either treated or not with Latrunculin A (siFIP1 n=60, siOCRL n=61) overtime.

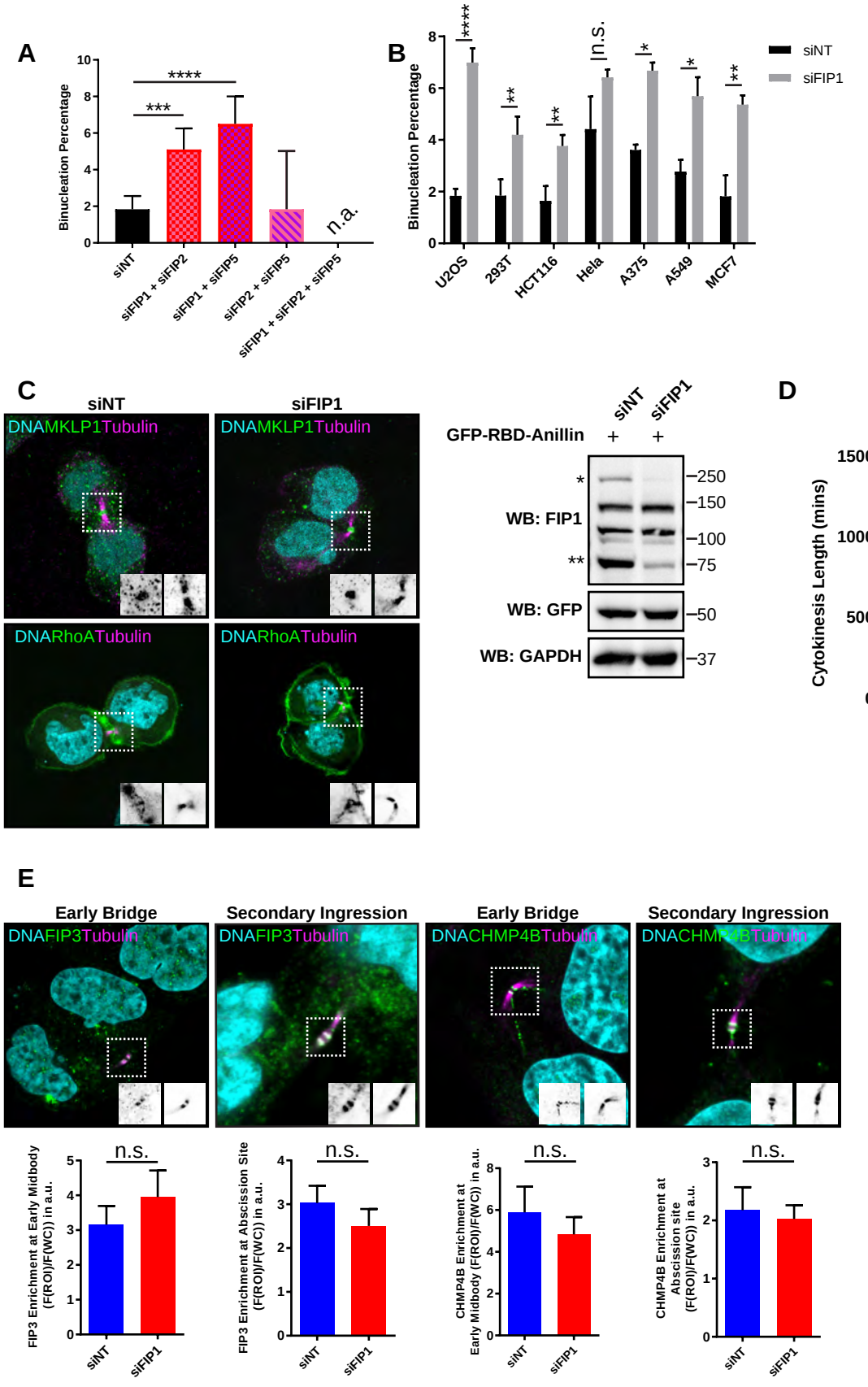

Fig S1. Supplementary information pertaining to figure 1

A) Quantifications of average cellular binucleation. siNT=504, siFIP1+siFIP2 n=90, siFIP1+siFIP5 n=15, siFIP2+siFIP5 n=27. P-value < 0.001 = ***, P-value < 0.0001 = ****, n.a. = unmeasurable, Two-tailed Student T-test. B) Quantification of cellular binucleation following depletion of FIP1 in indicated cell lines. siNT in U2OS, 293T, HCT116, A375, A549 and MCF7 respectively n=504, 230, 112, 175, 367, 378 and 100. siFIP1 in U2OS, 293T, HCT116, A375, A549 and MCF7 respectively n=766, 375, 137, 265, 447, 327, 200. P-value < 0.05 = *, P-value < 0.01 = **, P-value < 0.0001 = ****, n.s. = not significant, Two-tailed Student T-test. C) (Left) Representative images of cells treated with either siNT or siFIP1 wherein DNA is stained in cyan, β-Tubulin in magenta, and either (upper two panels) MKLP1 in green or (lower two panels) RhoA-binding-domain-of-anillin in green. Inverted black and white images of the green and magenta channels of MKLP1/RhoA-binding-domain-of-anillin and β-Tubulin are shown in the lower right corner zooms. Arrows indicate either the accumulation of MKLP1 at the midbody or the localization of RhoA at the midbody. (right) Representative Western blot showing FIP1 knockdown and GFP expression of the GFP-RhoA-binding-domain-of-anillin in both conditions. Note that FIP1 antibody has non-specific bands and single star denotes FIP1B, double star denotes FIP1C. D) Dot plot of every value for cytokinesis timing of indicated conditions corresponding to figure 1E and figure 1H. siNT n=70, siFIP1 n=133, siFIP2 n=70, siFIP1 + GFP-FIP1A n=18, siFIP1 + GFP-FIP1B n=55, siFIP1 + GFP-FIP1C n=62. Bars correspond to average value and upper and lower bars correspond to inter-quartile range. P-value < 0.0001 = ****, n.s. = not significant, Wilcoxon signed-rank test. E) Representative images of cells treated with either siNT or siFIP1 wherein DNA is stained in cyan, β-Tubulin in magenta, and either (left two panels) FIP3 in green or (right two panels) CHMP4B in green. Inverted black and white images of the green and magenta channels of FIP3/CHMP4B and β-Tubulin are shown in the lower right corner zooms. (lower) Quantification of either FIP3 or CHMP4B average fluorescence intensity signal enrichment in a ROI around the ICB, measured as the region of the β-Tubulin staining and surrounding area during FIP1 depletion in either early bridges or abscission sites. For FIP3 siNT n=14, siFIP1 n=14. For CHMP4B siNT n=23, siFIP1 n=21. Two-tailed Student T-test.

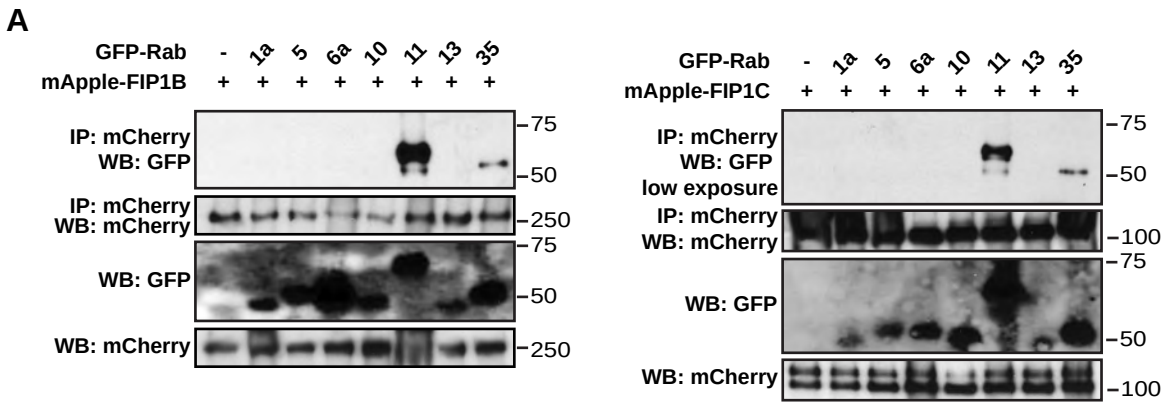

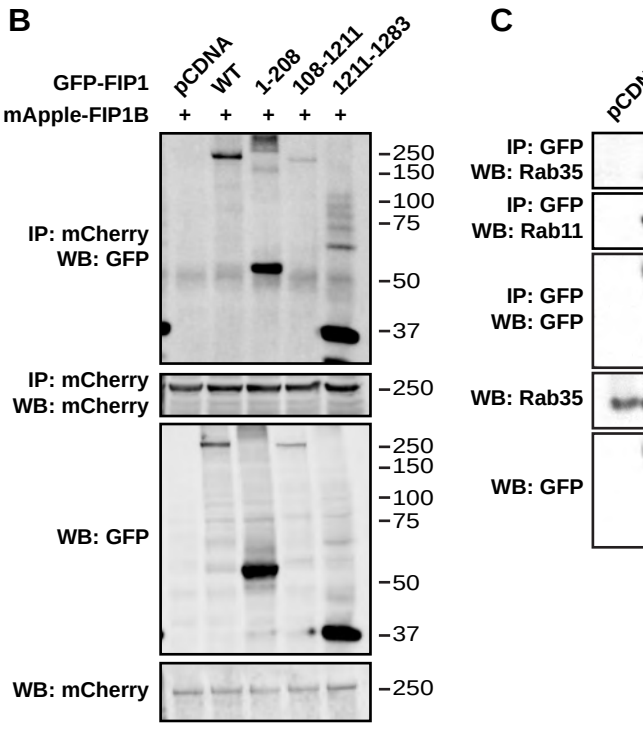

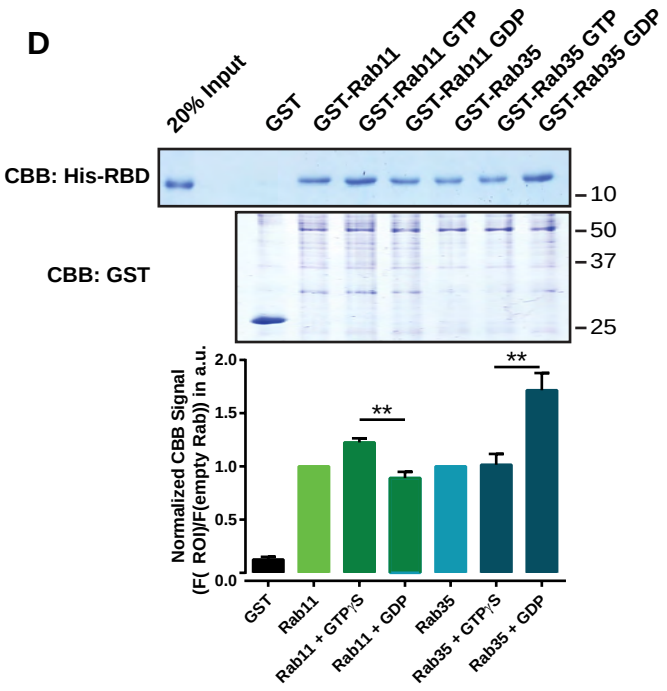

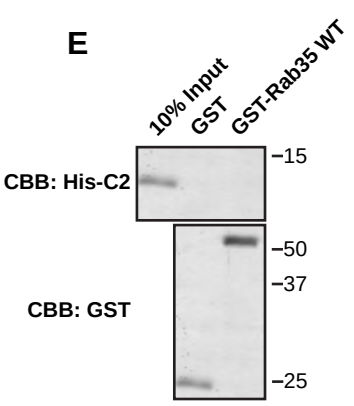

Fig S2. Supplementary information pertaining to figure 3

A) (left) Immunoprecipitation of GFP-Rab1a, GFP-Rab5, GFP-Rab6a, GFP-Rab10, GFP-Rab11, GFP-Rab13 and GFP-Rab35 by mApple-FIP1B (left) and mApple-FIP1C (right). B) Immunoprecipitation of FIP1 constructs from figure 3C baited to full-length mApple-FIP1B showing dimerization capacity for indicated domains. C) Immunoprecipitation of endogenous Rab35 or Rab11 by GFP-FIP1B or GFP-FIP1C. D) (upper) GST-pulldown of recombinant His-RBD by recombinant GST, GST-Rab11 or GST-Rab35 either loaded or not with GTP or GDP. (lower) Quantification of 4 independent GST-Rab pulldowns of His-RBD. P-value < 0.01 = **, Two-tailed Paired Student T-test. E) GST-pulldown of recombinant His-C2 by recombinant GST or GST-Rab35 and revealed by CBB staining.

A

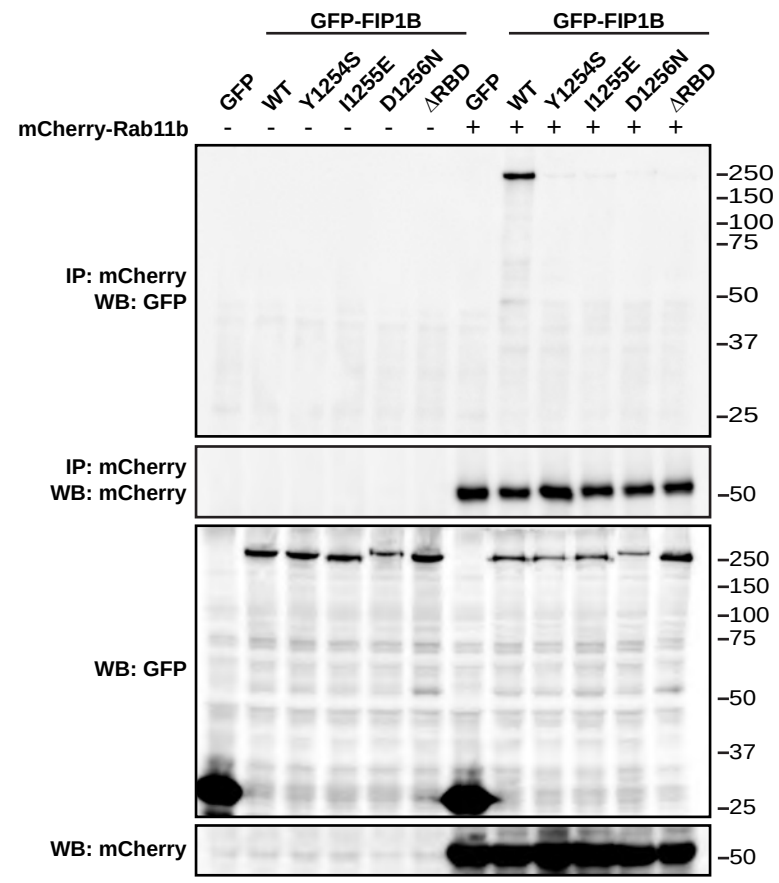

Fig S3. Supplementary information pertaining to figure 4
A) Immunoprecipitation of GFP-FIP1 RBD mutants by mCherry-Rab11b.

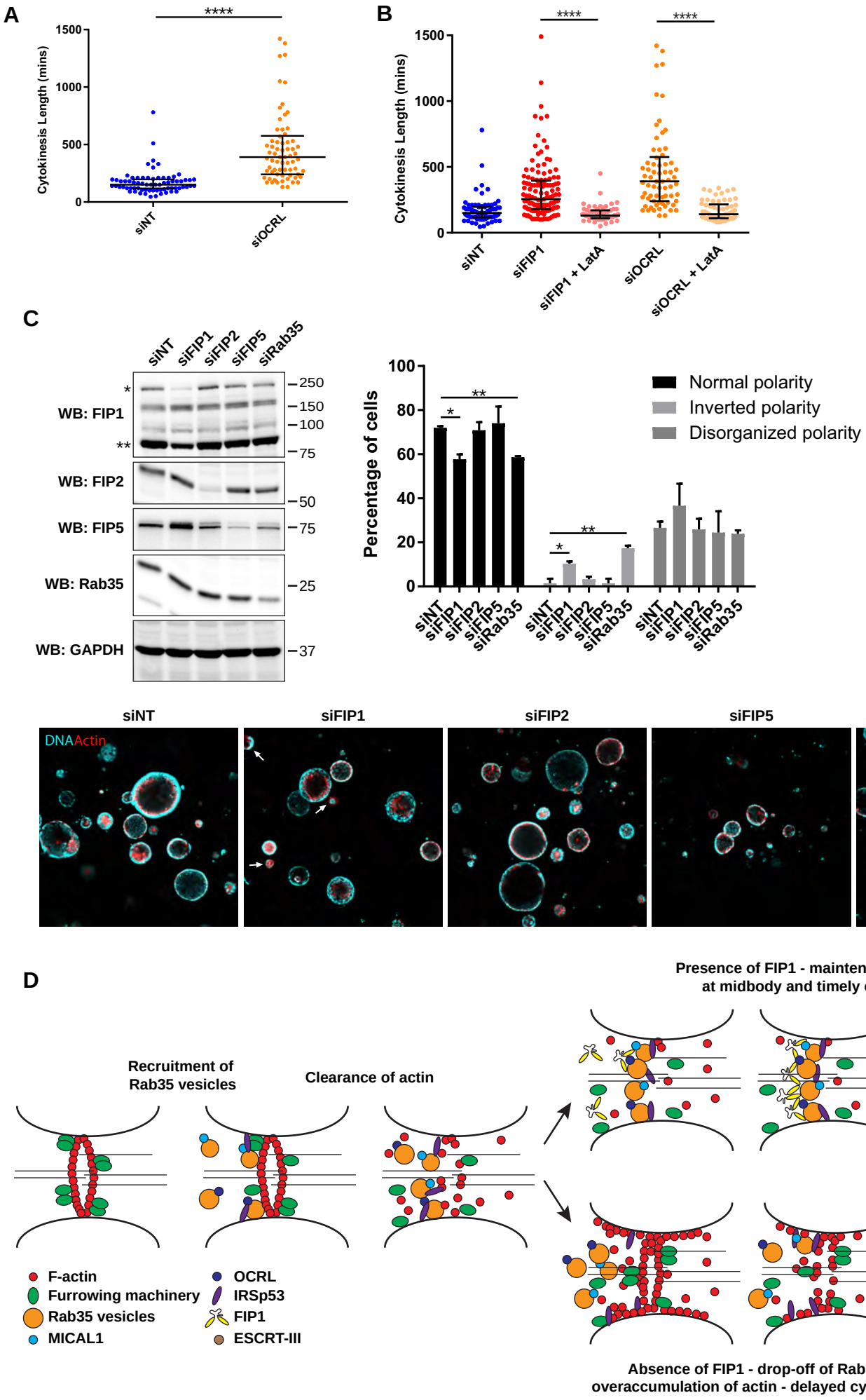

Fig S4. Supplementary information pertaining to figure 6

A) Dot plot of every value for cytokinesis timing of indicated conditions corresponding to figure 6B. siNT n=70, siOCRL n=70. Bars correspond to average value and upper and lower bars correspond to inter-quartile range. P-value < 0.0001 = ****, Wilcoxon signed-rank test. B) Dot plot of every value for cytokinesis timing of indicated conditions corresponding to figure 6E. siNT n=70, siFIP1 n=133, siFIP1 + LatA n=60, siOCRL n=70, siOCRL + LatA n=61. Bars correspond to average value and upper and lower bars correspond to inter-quartile range. P-value < 0.0001 = ****, Wilcoxon signed-rank test. C) (upper left) Western blot showing protein depletions after treatment with siNT, siFIP1, siFIP2, siFIP5 or siRab35. (upper right) Quantification of different polarities in each condition, either normal, inverted or disorganized polarity. siNT total n=116, siFIP1 total n=92, siFIP2 total n=126, siFIP5 total n=86, siRab35 total n=148. P-value < 0.05 = *, p-value < 0.01 = **, Two-tailed Student T-test. (lower) Representative images of single Z-planes of Caco-2 cysts depleted for indicated proteins. DNA is shown in cyan and Actin is stained in red. Arrows point to cells showing either complete or partial inverted polarity represented as Actin on the basal side of the cysts. D) Schematic representation of FIP1 function in cytokinesis.